◆ Human Brain Mapping 30:3865–3886 (2009) ◆

# Functional Segmentation of the Brain Cortex Using High Model Order Group PICA

**Vesa Kiviniemi,[1]* Tuomo Starck,[1] Jukka Remes,[1] Xiangyu Long,[1,2] Juha Nikkinen,[1] Marianne Haapea,[1,3] Juha Veijola,[3,5] Irma Moilanen,[4] Matti Isohanni,[3] Yu-Feng Zang,[2] and Osmo Tervonen[1]**

[1]*Department of Diagnostic Radiology, Oulu University Hospital, Oulu, Finland*
[2]*State Key Laboratory of Cognitive Neuroscience, Beijing Normal University, Beijing, China*
[3]*Department of Psychiatry, Oulu University, Finland*
[4]*Department of Child Psychiatry, Oulu University Hospital, Oulu, Finland*
[5]*Academy of Finland, Helsinki, Finland*

**Abstract:** Baseline activity of resting state brain networks (RSN) in a resting subject has become one of the fastest growing research topics in neuroimaging. It has been shown that up to 12 RSNs can be differentiated using an independent component analysis (ICA) of the blood oxygen level dependent (BOLD) resting state data. In this study, we investigate how many RSN signal sources can be separated from the entire brain cortex using high dimension ICA analysis from a group dataset. Group data from 55 subjects was analyzed using temporal concatenation and a probabilistic independent component analysis algorithm. ICA repeatability testing verified that 60 of the 70 computed components were robustly detectable. Forty-two independent signal sources were identifiable as RSN, and 28 were related to artifacts or other noninterest sources (non-RSN). The depicted RSNs bore a closer match to functional neuroanatomy than the previously reported RSN components. The non-RSN sources have significantly lower temporal intersource connectivity than the RSN ($P < 0.0003$). We conclude that the high model order ICA of the group BOLD data enables functional segmentation of the brain cortex. The method enables new approaches to causality and connectivity analysis with more specific anatomical details. *Hum Brain Mapp 30:3865–3886, 2009.* 

**Key words:** ICA; fMRI; resting state; brain cortex

## INTRODUCTION

Because the discovery of functionally connected low frequency fluctuations of the blood oxygen dependent (BOLD) with a functional MRI by Biswal et al. [1995], the detection of baseline activity within functional brain networks has become a fast growing interest area in brain imaging research [Fox and Raichle, 2007; Vincent et al., 2007]. Intracortical local field potential and multiunit activity fluctuations partly correlate with the fluctuations of the BOLD signal with a six second lag in anesthetized conditions [Logothetis et al., 2001; Shmuel and Leopold, 2008]. In addition to the electrophysiological activity, metabolic and vasomotor effects partly explain the detected changes

Additional Supporting Information may be found in the online version of this article.

Contract grant sponsor: Finnish Academy-Chinese NSFC Collaboration NEURO-Program; Contract grant number: 117111; Contract grant sponsor: Finnish Medical Foundation; Contract grant sponsor: Finnish Neurological Association.

*Correspondence to: Vesa Kiviniemi, Department of Diagnostic Radiology, Oulu University Hospital, Oulu, Finland.
E-mail: vesa.kiviniemi@oulu.fi

Received for publication 24 October 2008; Accepted 1 April 2009
DOI: 10.1002/hbm.20813
Published online 8 June 2009 in Wiley InterScience (www.interscience.wiley.com).

of BOLD fluctuation [Fukunaga et al., 2008; Kannurpatti et al., 2008; Kiviniemi, 2008].

The combined effects of these fluctuations in neuronal networks have been shown to be differentiable from noise during normal, awake resting conditions. Independent component analysis (ICA) is an effective tool in separating statistically independent source signals of the BOLD data. ICA separates various sources of the fMRI signal by maximizing the non-Gaussianity of the source signals. Spatial domain ICA (sICA) can separate BOLD signal sources that represent reactions to externally cued task-activations, background activity within functional brain (i.e. resting state) networks (RSN), and various physiological noise and artifact sources [Beckmann and Smith, 2004; Beckmann et al., 2005; Calhoun et al., 2001; Kiviniemi et al., 2003; McKeown et al., 1998; Van de Ven, 2004]. ICA methodology yields results that are equally accurate to other contemporary methods of detecting large scale temporally coherent networks from the BOLD signal data [Long et al., 2008].

It has been suggested that 10 to 12 RSNs can be detected from the brain cortex from resting state BOLD data, using ICA with a component dimensionality, i.e. a model order, around 25–40 components [Beckmann et al., 2005; De Luca et al., 2006; Damoiseaux et al., 2006]. However, the most recent reports on topographic delineation of cortex and functional connectivity nodes show that there should be more than a dozen detectable functional networks on the brain cortex [Bartels and Zeki, 2005; Cohen et al., 2008; Di Martino et al., 2008; Malinen et al., 2007; Mezer et al., 2009; Pawela et al., 2008]. When the model order of the ICA estimation is increased, the separated BOLD signal sources have been shown to split into several functional nodes [Li et al., 2007; Ma et al., 2007; Malinen et al., 2007; Eichele et al., 2008]. McKeown et al. [2002] have shown that the detected ICA components of BOLD data actually represent deterministic signal sources of the data, even in very high model orders.

In this study, we evaluate how many independent RSN signal sources of baseline brain activity can be detected from the brain cortex using a fairly large group of subjects and a relatively high order group ICA. We show that the previously detected RSN signal sources can be differentiated into a more finely tuned functional anatomy by extending the use of temporal connectivity, the frequency power spectral and the anatomical clustering characteristics of the signal sources into group analysis data. We show that over 60 of the detected signal sources can be robustly detected with repeatability analysis (ICASSO-software package: http://www.cis.hut.fi/projects/ica/icasso/) from group data. We found supporting evidence for our hypothesis that true RSN sources have increased temporal intersource connectivity compared to noise sources. Spatial overlap of the RSN components and predefined anatomical structures are presented. The possible functional and clinical implications of the results are discussed.

## MATERIALS AND METHODS

The ethical committee of Oulu University Hospital has approved the studies for which the subjects have been recruited, and informed consent has been obtained from each subject individually according the Helsinki declaration. Fifty-five control subjects were chosen (age 24.96 ± 5.25 years, 32 females, 23 males) from three resting state studies: a 1986 birth cohort study of ADHD and psychosis; brain tumor resting state study, total $n = 200$. Subjects were imaged on a GE 1.5T HDX scanner equipped with an eight-channel head coil using parallel imaging with an acceleration factor 2. The scanning was done during January 2007–May 2008. All subjects received identical instructions: to simply rest and focus on a cross on an fMRI dedicated screen which they saw through the mirror system of the head coil. Hearing was protected using ear plugs, and motion was minimized using soft pads fitted over the ears.

The functional scanning was performed using an EPI GRE sequence. The TR used was 1,800 ms and the TE was 40 ms. The whole brain was covered, using 28 oblique axial slices 4 mm thick with a 0.4 mm space between the slices. FOV was 25.6 cm × 25.6 cm with a 64 × 64 matrix, and a flip angle of 90°. The resting state scan consisted of 253 functional volumes. The first three images were excluded due to T1 equilibrium effects. In all three studies, the resting state scanning started the protocols, and lasted 7 min and 36 s. In addition to resting-state fMRI, T1-weighted scans were taken with 3D FSPGR BRAVO sequence (FOV 24.0 cm, matrix 256 × 256, slice thickness 1.0 mm, TR 12.1 ms, TE 5.2 ms, and flip angle 20°) to obtain anatomical images for co-registration of the fMRI data to standard space coordinates.

### Preprocessing of Imaging Data

Head motion in the fMRI data was corrected using multiresolution rigid body co-registration of volumes, as implemented in FSL 3.3 MCFLIRT software [Jenkinson et al., 2002]. The default settings used were as follows: middle volume as reference, a three-stage search (8 mm rough + 4 mm, initialized with 8 mm results + 4 mm fine grain, initialized with the previous 4 mm step results) with final trilinear interpolation of voxel values, and normalized spatial correlation as the optimization cost function. Brain extraction was carried out for motion corrected BOLD volumes with optimization of the deforming smooth surface model, as implemented in FSL 3.3 BET software [Smith, 2002] using threshold parameters $f = 0.5$ and $g = 0$, and for 3D FSPGR volumes, using parameters $f = 0.25$ and $g = 0$. After brain extraction, the BOLD volumes were spatially smoothed; 7 mm FWHM Gaussian kernel and voxel time series were detrended using a Gaussian linear high-pass filter with a 125 second cutoff. The FSL 4.0 fslmaths tool was used for these steps.

Multiresolution affine co-registration as implemented in the FSL 4.0 FLIRT software [Jenkinson et al., 2002] was used to co-register mean nonsmoothed fMRI volumes to 3D FSPGR volumes of corresponding subjects, and 3D FSPGR volumes to the Montreal Neurological Institute (MNI) standard structural space template (MNI152_T1_2mm_-brain template included in FSL). Trilinear interpolation was used, a correlation ratio was used as the optimization cost function, and regarding the rotation parameters a search was done in the full $[-\pi\ \pi]$ range. The resulting transformations and the trilinear interpolation were used to spatially standardize smoothed and filtered BOLD volumes to the 2 mm MNI standard space. Because an sICA was run later on fMRI data concatenated from the 55 subjects, in practice the spatial resolution of spatially standardized BOLD volumes had to be lowered to 4 mm.

## Spatial Domain Analysis

Analysis was carried out using probabilistic independent component analysis (PICA) [Beckmann et al., 2004] on preprocessed and spatially standardized BOLD data, temporally concatenated from data sets of individual subjects. The implementation of PICA and temporal concatenation in FSL 4.0 MELODIC software was used in this study. The default processing provided in MELODIC, and used in this study, starts on the subject level. Intensities of voxel time courses in preprocessed fMRI volumes are converted to percentages of change with respect to the mean intensity in those voxels. This is followed by group level joined normalization of voxel time course variances. The mean 4D fMRI data set is averaged from individual data sets, and the variance estimate is computed from it. The variance estimate used in normalization is computed so that (1) data with respect to its time points (temporal dimensions) is whitened, (2) in whitened space, large values corresponding to variance, possibly not originating from Gaussian processes, are noted with some threshold value, and their influence excluded from data in the original space, after which (3) variance is computed ordinarily on resulting residual data. Within MELODIC implementation and in its joined normalization scheme, this threshold value was set to 3.1. Fourth, voxels with insufficient variances ($<0.0001$) are set to zero because they contain nearly constant time courses, and in that sense a bad signal-to-noise ratio that would (after variance normalization) contribute too much to the analysis. Each individual subject fMRI data set is divided voxel-wise with a standard deviation corresponding to the voxel-wise variance estimate. A whitening matrix corresponding to the whitening mean 4D fMRI data set is computed and used for group-level joined whitening and dimensionality reduction of each individual subject fMRI data sets. The number of resulting dimensions corresponds to the model order of ICA that is intended to be used. In this study, the model order was chosen to be 70, in correspondence to the high order sICA modeling of the resting state BOLD data. Because PPCA estimation suggested 73 components in an initial test, we reduced it to 70 components due to better extraction of extracranial voxels after using a more sensitive BET algorithm outside the MELODIC framework.

The jointly whitened and reduced individual fMRI data sets are further whitened, and then temporally concatenated. Further dimensionality reduction is performed with principal components analysis (PCA) on the concatenated data. The number of dimensions in the concatenated data (number of subjects times 70) is reduced to the number of independent components to be computed, 70 in this study. Finally, FastICA [Hyvärinen, 1999] is performed using voxel values as samples, and PCA reduced and whitened temporal dimensions as variables. In this study, we used the default settings in the MELODIC software: symmetric orthogonalization and skewness ("pow3") as the contrast function.

In a PICA framework, estimated intensity maps (independent components) are converted to $Z$-scores by dividing intensity values by voxel-wise standard deviations of noise distribution. Standard deviations are estimated through calculation of corresponding voxel-wise variances of the original preprocessed data in the subspace left out by dimensionality reduction steps. Probability distributions of values in individual resulting score maps are modeled using a mixture of functions, a zero mean Gaussian function and two gamma functions. The Gaussian function corresponds to the effects due to chance, and the gamma functions model outliers not observed by chance. For a given $Z$-score, the sum of gamma function values divided by the sum of all function values can be used to calculate the probability of actually observing an effect with that score. With regard to these probabilities, a probability threshold ($P$-value) is set to leave out (set to zero) those voxel values in score maps that are presumed to be observed in the PICA results by chance. In this study, we used $P = 0.5$, attributing equal relevance to both false negatives and false positives.

The Juelich histological atlas [Eickhoff et al., 2007] and the Harvard-Oxford cortical and subcortical atlases (Harvard Center for Morphometric Analysis) provided with the FSL4 software package were used to quantify anatomical characteristics of thresholded $Z$-score maps. For this purpose, maps were upsampled back to 2 mm resolution MNI standard space. Individual anatomical regions in the probabilistic atlases were binarized and used as masks to extract the corresponding regions in maps. An FSL4 fslstats tool was used to calculate mean and maximum intensity in regions, as well as the location of maximum intensity. The number of voxels in the masked PICA maps was also calculated, and divided by the number of voxels in the whole anatomical masking region, to provide a percentage of the coverage of different anatomical areas by individual maps.

A neuroradiologist (VK) depicted the thresholded PICA maps corresponding to the RSNs by choosing anatomically

clustered sources in the cortical regions, in the vicinity of functional brain regions. The sources were further classified into three regions for illustration purposes with a scheme modified from Salvador et al. [2005] (peri-sylvian = rolandic and temporal, frontal, occipito-parietal). In each of the selected sources (1) sources presented clustered voxel groups, (2) sources were focused on cortical structures, and (3) time courses in the ICA mixing matrix corresponding to the maps showed elevated low frequency (<0.1 Hz) power. Artifactual non-RSNs were identified based on their motion-related location at the borders of the brain, in cerebrospinal fluid (CSF), at the proximity of large blood vessels, in white matter, and in the vicinity of areas shown to be susceptible to physiological pulsations with relatively increased or mixed high frequency power [Birn et al., 2006; Lund et al., 2006].

### Repeatability Analysis

The data from the final step prior to FastICA was also subjected to ICA repeatability analysis (ICASSO) [Himberg et al., 2004]. Because ICA is sensitive to its initialization, this framework runs FastICA multiple times on the same data, with random initializations and clusters with a hierarchical clustering algorithm, on the results from individual runs. The number of clusters is the same as the number of components and provides statistics about the quality of the clusters, reflecting the stability of the ICA results. In this study, we used the provided Matlab implementation [Himberg et al., 2004] with 100 runs, and a low epsilon threshold (0.0000001) so that optimization would not converge too soon before reaching extrema. Symmetric orthogonalization and skewness ("skew") as the contrast function were also used in this setting. The conservative cluster quality index $I_q$ was used to estimate individual component repeatability [Himberg et al., 2004]. $I_q$ is one for an ideal cluster, and decreases when component clusters become less compact and isolated in repeated ICA runs.

### Time Domain Analysis

A mixing matrix estimated in an sICA contains time courses corresponding to estimated spatial maps (independent components). The time courses represent the behavior of nonartifact components in time more accurately than the average BOLD time courses computed from the same spatial area as in the maps; this is because the most dominant effects of cardiac, respiratory, CSF-pulsation and motion, and other artifacts are eliminated into separate components. This offers preprocessed time courses for temporal correlation analysis of BOLD signal sources [Jafri et al., 2008; Sorg et al., 2007].

In a temporal concatenation scheme, the mixing matrix can be divided into subject specific consecutive segments, reflecting subject-wise temporal behavior of components. In this study, these subject specific 250 point time courses were used to assess pair-wise inter component connectivity on the group level. The time courses were first detrended, and then correlated with each other on the subject level with the Pearson product–moment correlation coefficient with a zero lag. The group level average and standard deviation of the results were calculated for each correlation pair's absolute values.

In addition, the mean of these group-level absolute correlation coefficients was calculated per component within the group of components corresponding to RSNs, and within the group corresponding to non-RSNs. These values were tested for differences with a two-sample *t*-test between RSNs and non-RSNs.

### Frequency Domain Analysis

The subject-wise time courses extracted from the mixing matrix were (after detrending) also converted to power spectra, to assess contribution of low frequency power in them. For each time course, a spectrogram was computed with 128-point rectangular windowing in Matlab (R2008a) with the similarly named function. Rectangular windowing was sufficient, because no sinc-interpolation (e.g. no zero padding) was used in the Discrete Fourier Transform. The absolute values of the resulting 123 spectra were raised to the second power to approximate power spectra, and they were averaged to obtain a final power spectrum estimate for each time course.

For the group-level analysis, each power spectrum was normalized by dividing its values by its total power. Normalized power spectra from individual subjects were averaged for each component, to produce a group-level representation of temporal power. In addition, Singular value decomposition was used for each component to produce, on a group-level, a rank-1 approximation of subject-specific power spectra for that component. Rank-1 approximation depicts frequencies with the most commonly elevated power in subject-level time courses.

## RESULTS

### Repeatability Measures

An ICASSO algorithm was run on the pre-whitened PCA-data matrix provided by the MELODIC. After 100 repeated runs of the group ICA, significantly clustered components were detected. Fifty-one of the 70 ICs had an $I_q$ over 0.8, and 60 ICs still had an $I_q$ of at least 0.7. Figure 1 shows clustering of the centroid components and stability indexes in reducing the stability order. PICA estimation of the group data yielded 73 components. We made seven separate runs altering the basic spatial smoothening parameters (3–7 mm FWHM), temporal high (100–420 s) and low-pass filtering. In essence, the spatial correlation

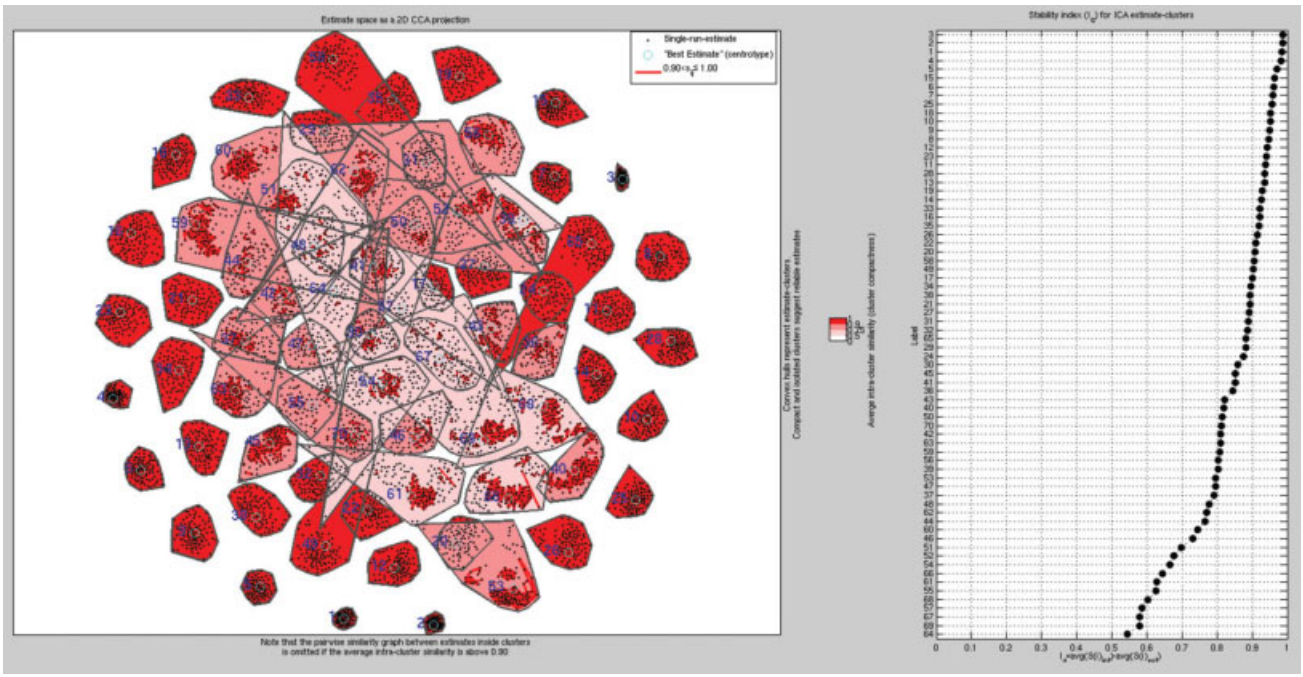

**Figure 1.**

On the left, the clustering of group PICA-derived components in ICASSO after 100 repeated runs. On the right, ICASSO run components in descending clustering index values, showing that in 60/70 components the clusters are repeatedly detectable ($I_q \geq 0.7$). Please note that the ICASSO cluster numbers are not the same as the PICA numbers in the text and other images.

between the detected ICA components of separate runs was always >0.7.

## RSN-Identification

The group PICA separated 42 components that were identified as RSN. These 42 components cover most of the brain cortex excluding areas having susceptibility artefacts due to air sinuses. The corresponding RSN components had an average $I_q = 0.83$ ($\pm 0.13$) in the ICASSO analysis. The RSN components had elevated low frequency fluctuation power and, spatially, were clustered components located in the cortex. Figures 2–4 show fused maps and separate spatial distributions of 25 of the different signal sources on both sides of the Sylvian fissure and the central sulcus (peri-sylvian), in the frontal lobe (frontal), and in the occital and parietal regions (occipito-parietal). The remaining signal sources are shown in Figure 5 in more optimal 3D presentations.

Twenty-eight ICs were related to non-RSN sources. Eighteen non-RSN components were identified as motion/realignment artifacts, and physiological noise sources such as arterial and CSF pulsation. Ten of the discarded components were detected as large voxel clusters in the white matter and were not further analyzed. Ten examples of the non-RSN sources are shown in Figure 6.

## Anatomical Parcellation

In practice, most of the cerebral cortex can be shown to be segmented with the IC components (c.f. the upper rows in Figs. 2–4). On average, the *maximal* spatial correlation between detected RSN components and other sources was 0.2 (SD 0.04). This can be seen in Figures 2–4 as a limited spatial overlap of separate signal source components. Table I lists the first three to five largest overlapping *anatomical* segments used in FSL4 (Juelich and Oxford atlases) in comparison with the selected RSN signal sources. The RSN components actually show more connectivity nodes to multiple other anatomical structures, and the complete table is presented in the Supporting Information material (Supporting Information Table I.2). In the following, the individual RSN sources are evaluated, based on spatial overlap with preexisting anatomical segments. Temporal intersource synchrony of the sources and the highest spatial correlation with ICASSO components are also presented.

## Rolandic Signal Sources

Figure 2 shows six signal sources identified as perirolandic, situated at or in the vicinity of the central sulcus. Although most of the sources have strong localized connectivity, some have long range connectivity to other primary and secondary sensory areas, such as to the visual and auditory regions.

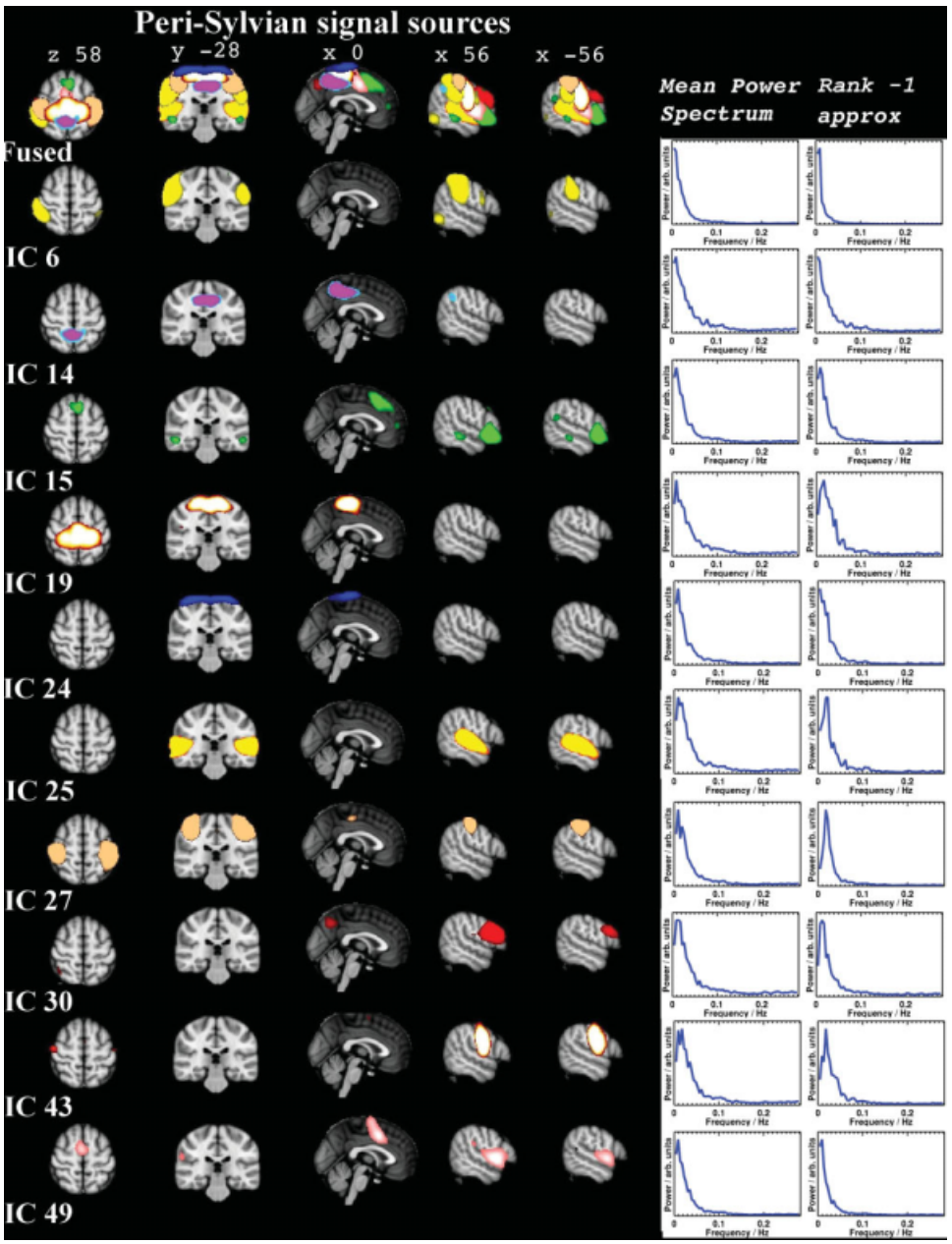


**Figure 2.**

Signal sources located around the Sylvian fissure, both peri-rolandic and temporal sources are presented. At the top, a fused image presenting overlays of the different sources. Below that, IC sources are mapped with color labels provided by the fsl-view tool. On the right, the mean power spectra and rank 1 approximate on the same row as the map of the given source. On the left, the sources are numbered using the same numbers as referenced in the text.

The motor cortex was divided into two different signal sources resembling the classical separation of upper cortical structures representing the hand areas (IC 27) and midline feet areas (IC 19). Similar to the original discovery of Biswal et al. [1995], there was a midline connectivity node posterior to the typical SMA seen during activation studies. Another motor cortex component, IC 24, was depicted, but it was not clear whether such parcellation is due to physiological factors, or if the results are split due to positioning differences in the original BOLD axial slices.

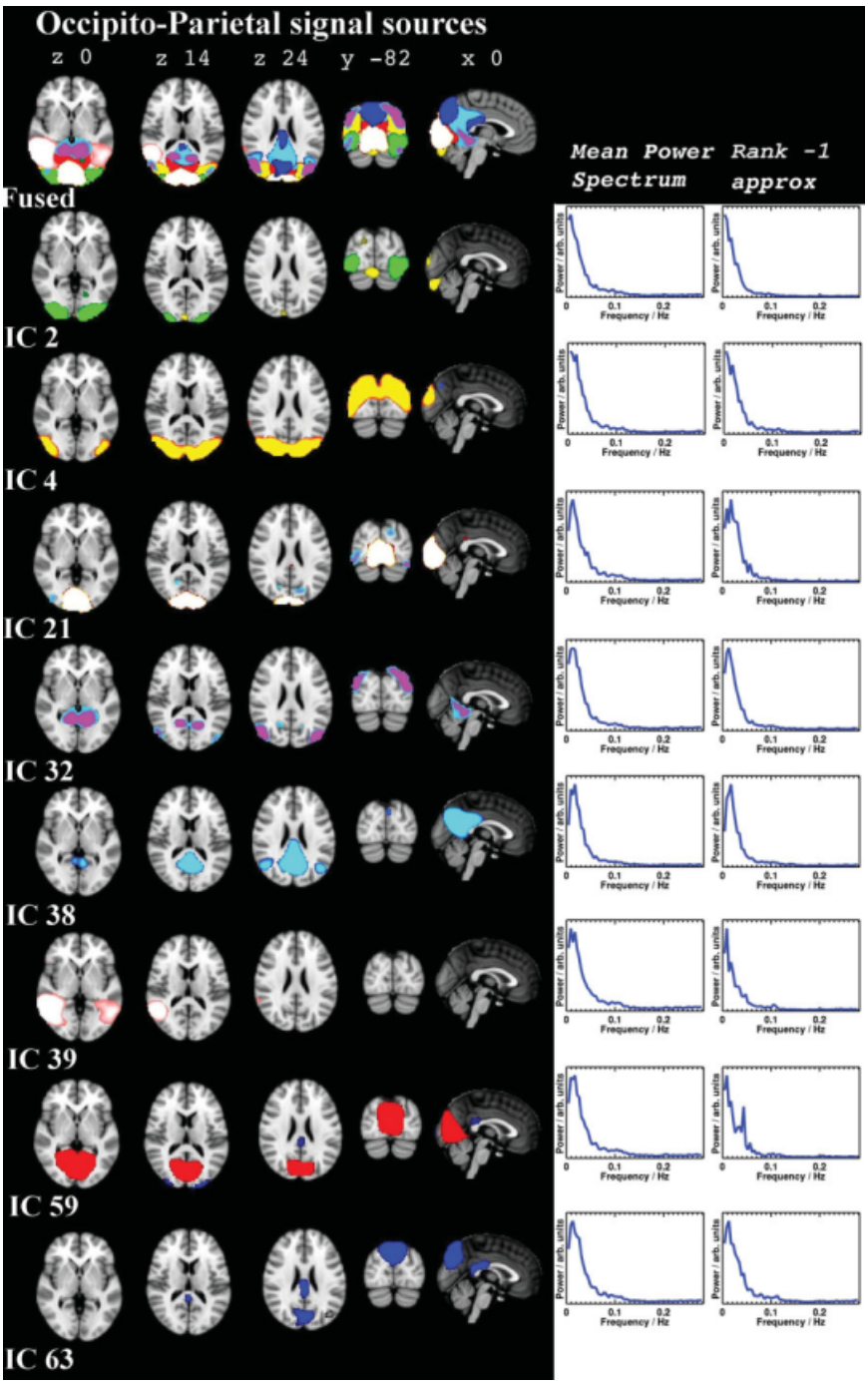


**Figure 3.**
The occipital and parietal RSN signal sources presented in the same way as in Fig. 2 with power spectra and rank 1 approximates. The DMN posterior part is depicted in IC 38.

Anterior to motor areas there were unilateral components (ICs 53 and 60) with positive connectivity to the cerebellum. The right anterior motor IC 60 was spatially larger than the left IC 53.

Primary and secondary somatosensory cortices were separated into signal sources of their own (IC 6 and, 43, respectively). Posterior to these, there was a symmetrical, bilateral post-somatosensory cluster (Fig. 5, IC 40). The somatosensory signal source also showed smaller clusters of connectivity to anatomical visual, auditory and Broca's areas (c.f. Supporting Information Table I.2). The signal source IC 14 was situated below the somatosensory cortex in the white-gray matter boundary. The secondary somatosensory source (IC 43) also showed connectivity with

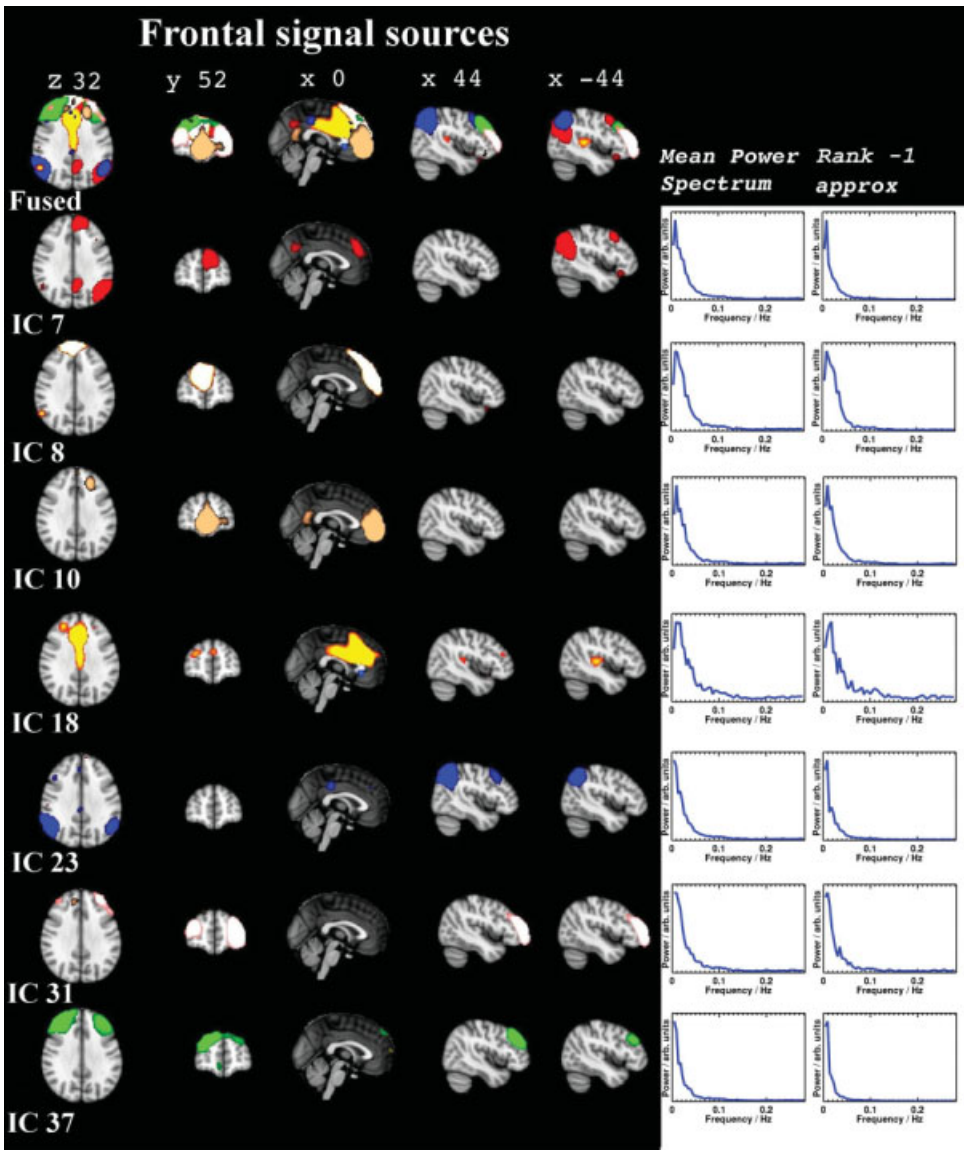


**Figure 4.**

Examples of frontal signal sources in a similar order to Figures 2 and 3. Note the relative lack of power peaks compared to the more posterior components. The default mode network pattern can be seen to originate from several subnetworks in the fused images at the top.

structures in the cerebellum, in addition to secondary somatosensory, auditory, motor, and premotor anatomical structures. The supplementary motor area (SMA, i.e. juxtapositional lobule) area had bilateral connectivity clusters in IC 49, primarily involving the insular cortices, and partly involving the secondary somatosensory area, resembling mirror neuron networks. Interestingly, both premotor areas BA6 also presented unilateral components, i.e., ICs 53 and 60 (see Fig. 5). There was a tendency that the farther the source was from the central sulcus the longer the distances were between detected connectivity clusters.

## Temporal Lobe Signal Sources

In Figure 2, the primary auditory cortex was identified as a bilateral component of its own, with a right brain dominance (IC 25). As with the peri-rolandic sources, this large network presented connectivity with other sources in distant regions, in both the motor and visual areas. A Broca's area on the left and an homologous right hemisphere Broca's area were detected in a unique bilateral component, with a clear, functionally connected cluster in the right paracingulate areas, posterior cingulate gyrus, and

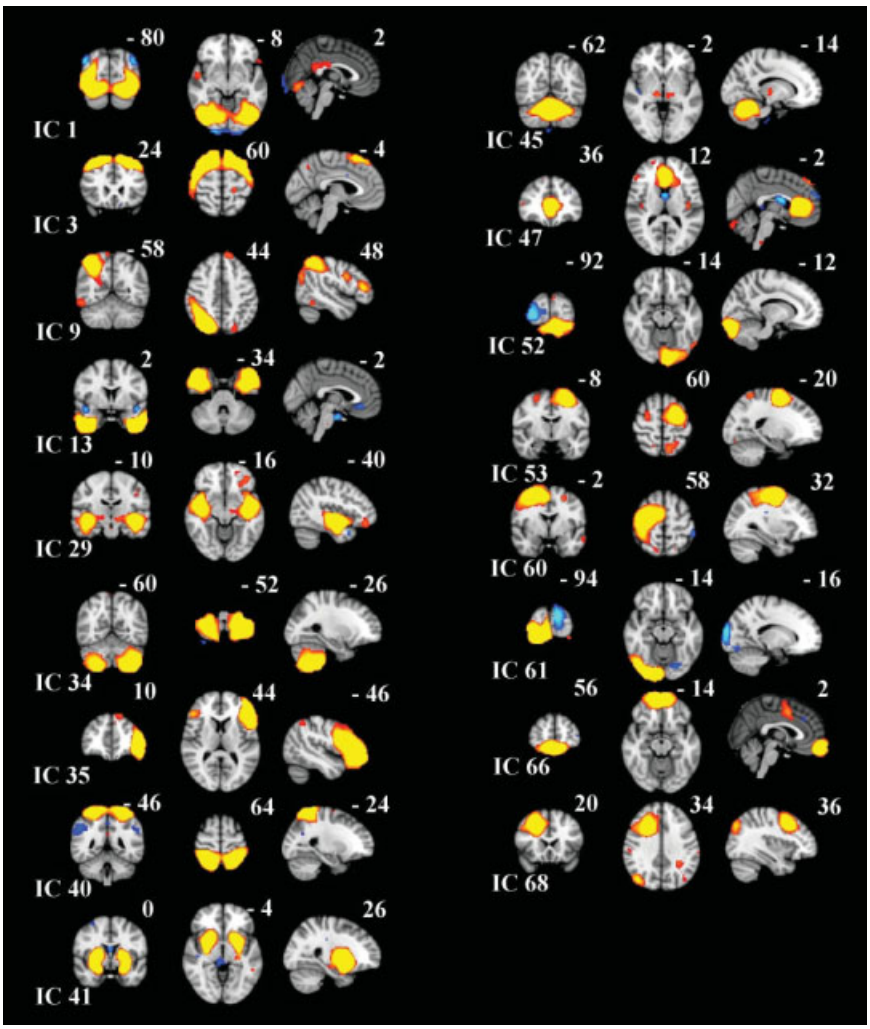


**Figure 5.**
Examples of the remaining 17 RSN in coronal, axial, and sagital views on an MNI template. The MNI coordinates are shown in the image. Red-yellow positive *Z*-scores, and blue negative *Z*-scores.

bilateral occipital poles (IC 30). The fronto-insular cortex of the salience network was detected in a bilateral IC 15 with a partial Broca's area and inferior frontal gyrus involvement, in addition to paracingulate gyrus connectivity [Shihadran et al., 2008]. IC 49 showing connectivity to SMA could be differentiated from the salience network. The temporal poles (IC 13, Fig. 5) were also detected in a unique signal source, with connectivity to midline structures to bilateral hippocampi.

### Frontal Signal Sources

The frontal lobe had 11 RSN signal sources, seven of which are presented in Figure 3. In five sources (ICs 7, 10, 18, 31, and 37), connectivity to language-related areas, such as the auditory cortex, inferior frontal gyrus, and/or Broca's anatomical areas, was detected. In addition to these areas, IC 7 and 10 were also connected to the anterior cingulate and paracingulate gyri. IC 7 had connectivity to the angular gyri and the visual cortex. IC 10 was present at the lower frontal pole and medial frontal cortex, and IC 8 was related to the upper frontal pole, and the middle and superior frontal and angular gyri. IC 18 was connected to the superior frontal gyrus, paracingulate, and cingulate gyri. IC 23 was connected to the angular and supramarginal gyri, along with the visual cortex. IC 37 was related to the superior and medial frontal gyri and the paracingulate gyri.

### Occipital and Parietal Signal Sources

There were seven separated signal source clusters in the occipital lobe, all spatially connected to visual areas (c.f. Fig. 4). IC 2 was situated at the lateral part of the primary visual cortex (V1), as in the lateral visual component in previous papers. Above and lateral to it was IC 4, with midline connectivity in V5. IC 39 was also comprised of bilateral V5 areas, yet different V5 areas from those in IC 4, with connectivity to V1 and 2 and the inferior and medial temporal gyrus. IC 59 typically presented the

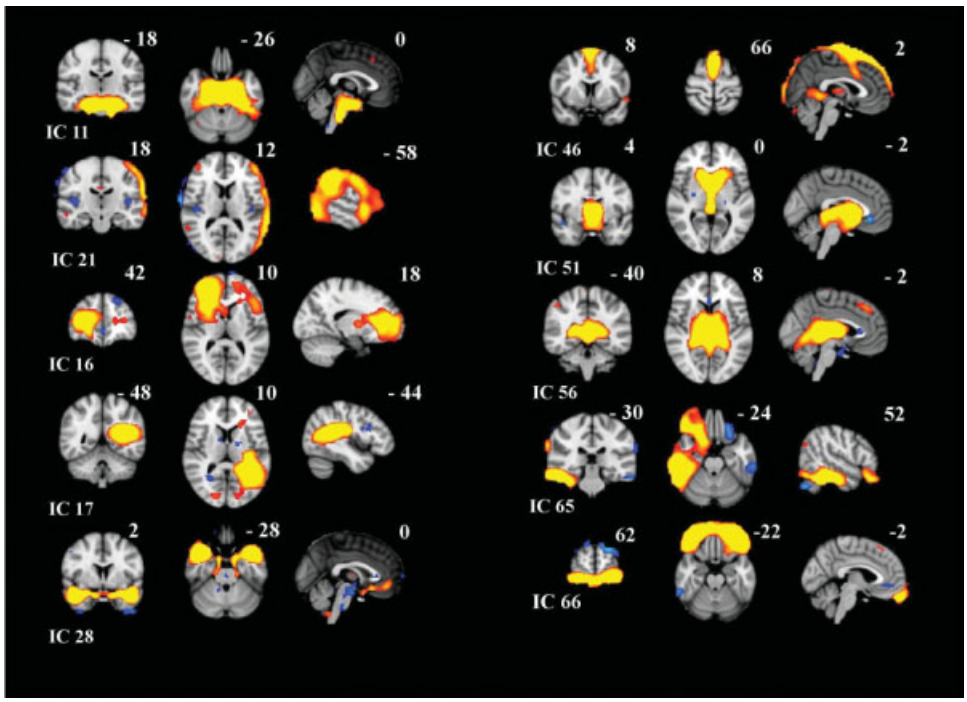


**Figure 6.**

Ten artefactual non-RSN sources, from top left: brain stem pulsation (IC 11), motion artefact (IC 18), two white matter sources (ICs 16 and 17), cerebral artery related (IC 28), sagital sinus (IC 46), two CSF-ventricle pulsation sources (ICs 51 and 56) and temporal motion-related source (IC 65) and frontal sinus susceptibility artifacts (IC 66).

previously detected medial visual RSN, comprising almost completely of the intracalcarine and supracalcarine cortex, the lingual cortex, and the major parts of V1 and 2 and the cuneal cortex. An anterior medial visual component IC 32 in V2, with hippocampal and geniculate body connectivity, was also detected. A posterior component IC 21 was separated from the medial central IC 59. The cuneal and precuneal cortex was dominant in IC 63, along with V1&2, with clear retrosplenial connectivity. In addition, there were two anticorrelated components in the visual areas (ICs 52 and 61) showing positive *Z*-scores caudally on the other visual cortex, and negative *Z*-scores on the contralateral side more cranially.

## Default Mode and Frontal Attention Control Sources

Several ICA sources were detected in the areas known to be related to the default mode network (DMN). IC 10, ventromedial prefrontal cortex (vmPFC); IC 38, precuneus and parietal lobule (PCC). ICs 7, 10, 23, 18, and 37 were closely related to anatomical structures of the DMN (c.f. Figs. 3 and 4). The regions usually detected as anti-correlated to DMN in correlation analysis were also detected as sources of their own, i.e. ICs 6, 40 and 49 [Fox et al., 2007; Buckner et al., 2008]. IC 17 resembles the frontal areas central executive network [Shihadran et al., 2008]. Figure 7 shows an example of PICA images calculated with 100 repeated ICASSO runs with model orders 10, 70, and 150. Note how the core areas of the default mode divide into smaller subnetworks with increasing model order.

## Time Domain Synchrony

The intersource connectivity between all the calculated ICs are presented in a matrix in Figure 8. The graph shows how the individual sources are connected to the other sources on average with zero time lag. The correlation coefficients range from 0.64 to −0.66 (±0.21). The mean correlation coefficients of each component provide an overall assessment of general intersource connectivity of a given IC. The overall connectivity of the non-RSN sources was statistically significantly lower than the connectivity of the RSN sources ($t = 4.6$, $P < 0.000024$, c.f. Fig. 8 bottom). Eight out of the 10 lowest values of summed correlation were depicted in non-RSN sources. There is, however, some overlap in the correlation values between the RSN and non-RSN sources, and temporal zero-lagged correlation alone cannot be used to separate the sources with absolute certainty.

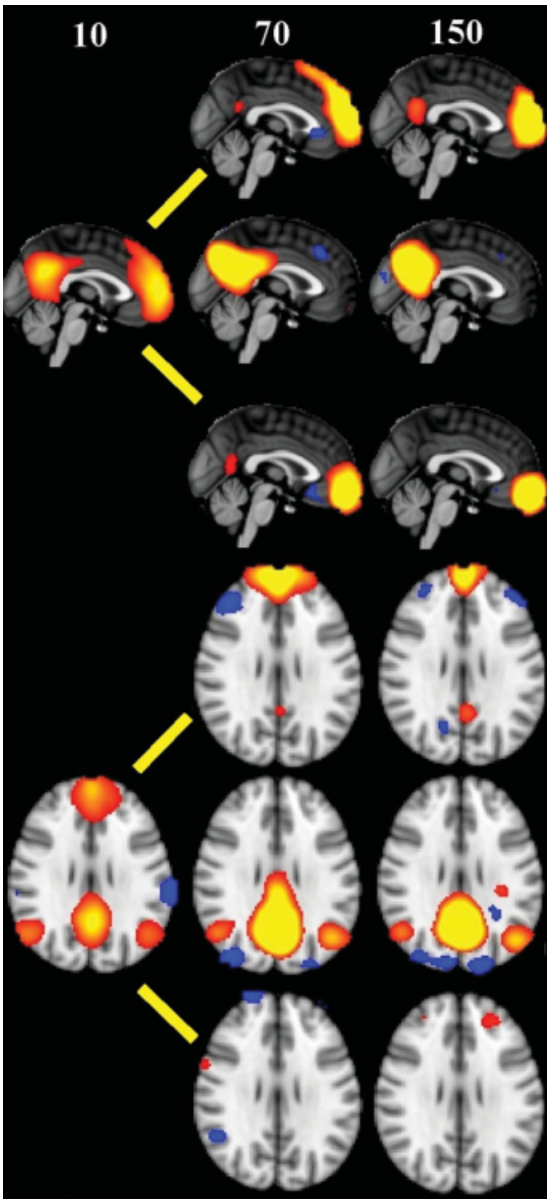


**Figure 7.**
Sagital and axial examples of the default mode network shown with model order 10, 70, and 150 after 100 ICASSO runs shown in a PICA setting in fsl4, with $P = 0.5$ threshold. The core default mode areas become separated into at least three independent subnetworks, one in the precuneus and posterior parietal areas, and two in the ventromedial prefrontal areas.

## Frequency Domain

The mean power spectra of the individual ICA time courses extracted from the group data mixing matrix had increased low frequency power with $1/f$ distribution characteristics (see also Figs. 2–4). The first rank approximate of the power spectra shows the most contributing frequencies, mostly presenting the same proportional distribution as the mean power spectra. In the majority of the components, the dominant feature is the $1/f$ characteristic trend. However, in ICs 7, 18, 19, 21, 25, 27, 30, 32, 38, 43, 59, and 63, there is a distinct peak in lower frequencies. That is, the lowest frequency is not with the largest power. The peaks were almost absent from frontal sources, with the exception of DFM related IC 18. Primary auditory IC 25,

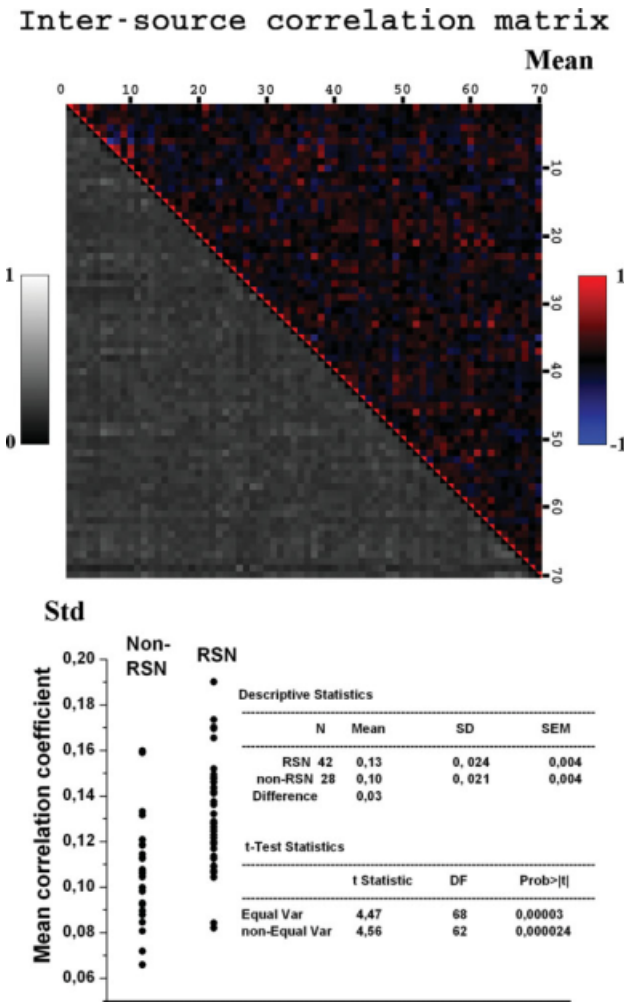


**Figure 8.**
Top: the individual correlation matrix of each signal source compared to each other enables assessment of the intersource connectivity of basically the entire brain cortex. Mean correlation coefficients with 0 time lag are color encoded at the top/right, and standard deviations of individual source correlation pairs in gray scale at the bottom. Below: mean inter-component correlation coefficients between individual sources are analyzed at the subject level. The RSN components show increased intersource connectivity between all the calculated sources compared to artifact related non-RSN sources.

somatosensory IC 43, motor ICs 19 and 27, and visual sources 21, 32, and 59 showed peaks. In the visual cortex, IC 59 in the medial areas had an exceptional 0.045 Hz frequency peak at the most dominant approximate. Default mode IC 38 and the Broca area source IC 30 also presented peaks in their power spectra.

## DISCUSSION

The results of this study represent functional segmentation of the human brain cortex, using the statistical independence of spontaneous brain activity sources as a delineating feature. We have shown that the intrinsic baseline activity of the brain cortex can be separated into 42 independent sources, having RSN features, using a high model order PICA approach. These sources cover virtually the whole brain cortex, excluding the sources affected by susceptibility artifacts near air-sinus interfaces. The dominant low frequency power characteristics of rank-1 approximate in the RSN support the idea that the sources represent low frequency background activity of the RSN. All of the RSN sources have increased LFF power in the mean power spectra (c.f. Figs. 2–4).

The utilization of continuous in vivo baseline activity information on brain activity offers a complementary method to previous anatomical/histological dissection studies, as well as imaging data-based segmentation studies, which currently form the basis of spatial localization schemes. The introduction of functional segmentation offers a more accurate tool for delineating functional activity that traverses presently used tissue segmentation borders in connected neuronal networks. In addition, these IC source maps can be used as data driven, statistically independent, functional seed regions for further correlation analyses.

Using present 1.5-T MRI scanning methodology our group has identified 42 signal sources over the whole brain cortex. The results of this study are in excellent agreement with the recent results of Cohen et al. [2008], who showed several small functionally connected areas within the same cortical regions. The work of Malinen et al. [2007] convincingly shows that during natural stimuli there are all together at least 20 task- and nontask-related signal sources detectable in the brain. Compared to a higher resolution fMRI scan on a rat, the results of this study seem conservative, because rats were shown to have some 20 connectivity hubs detectable in the somatosensory and visual systems alone [Pawela et al., 2008]. Two groups have been able to identify separate regions from the striatum and thalamus with distinct functional connectivity to the brain cortex in human subjects [DiMartino et al., 2008; Mezer et al., 2009]. On a submillimeter scale, anatomical structures of the visual field columns and cortical layers can be identified based on the spontaneous electrophysiological activity of subsecond time scales. This suggests that an even greater number of spontaneous signal sources will be detectable with increased spatiotemporal accuracy in the future [Kenet et al., 2003; Pelled and Goelman, 2004].

The previously detected 12 signal sources that were found in smaller datasets are basically summations of some of the sources presented here [Beckmann et al., 2005; Damoiseaux et al., 2006; Sorg et al., 2007; Jafri et al., 2008]. An example of this can be seen in the Figure 7, where the DMN is initially presented as one single source with the model order 10, and, after increasing the model order, becomes divided into several sources. It seems that low model orders provide information on large scale networks, whereas higher model orders, at least in group-data settings, provide subnetwork accuracy. We are currently analyzing the effect of model order on the dividing of RSN's into subnetworks. We suggest that the 42 group-PICA signal sources depicted in this study represent a more finely-tuned and segmented version of the functional neuro-anatomy of the RSN's in the brain cortex, and therefore we strongly support using high model order in large group datasets.

The distinction of components into two categories of either RSN or non-RSN may be somewhat arbitrary although there have been some successful attempts towards automated noise removal that basically also delineates ICs into neuronal and artifactual originated ones [De Martino et al., 2007; Tohka et al., 2008]. One might justifiably speculate in the absence of definite exclusion criteria that there exist a "borderline" between RSN sources and non-RSN sources. Some ICs have features of cortical signal source overlapping with regions often presenting artifacts. For example ICs 3, 24, and 40 all are situated within the cranial brain cortex and somewhat resemble sources seen in individual ICA results as motion artefact/partial volume effects. However, at least ICs 40 seems to be a RSN based on further studies not shown here. On the other hand, ICs 8, 52, and 61 are situated very close to sagital or transverse sinuses and one might speculate that the source has some contribution from pulsation from sagital sinus. However, the sagital sinus at least was shown to have an even more confined source of its own (IC 46; c.f. Fig. 6). It would be beneficial to obtain a more quantitative criterion than anatomical positioning and low frequency fluctuation of the sources to differentiate true RSN sources from artefacts.

The signal sources depicted here accurately follow the known functional anatomy of the sensory and motor networks. Sources IC 19 and 27 together cover 89% of the right and 86% of the left primary motor cortices when compared to MNI atlases in fsl4. Primary sensorimotor areas were shown to have spatial connectivity with 14 ICs, 12 of which were the same (ICs 3, 4, 6, 14, 19, 24, 27, 40, 43, 53, 60, 66). The M1 anatomical area was uniquely connected to ICs 41 and 45, while S1 was connected to IC 9 and 35 (c.f. Supporting Information Table I.2). Somatosensory S1 had a spatial overlap of 61% (IC 6) and S2 72% (IC 43). The supplementary motor area (i.e. juxtapositional lobule) activity was differentiated from the primary

sensorimotor components, although it was shown to have connectivity to them. SMA was shown to be connected to 12 RSNs, the largest share being detected in IC 49 (58%). Also IC 53 (24%), IC 60 (34%), IC 18 (30%), and IC 19 (36%) had relatively high spatial overlaps with the SMA template. The unilateral and somewhat anterior pre-motor sources (ICs 53 and 60: Broadman area BA6, 42% and 55%, respectively) could be related functional differences of the subjects premotor areas [Longcamp et al., 2005].

Visual sources are separated into multiple sources, and not only into medial and lateral components as before. The primary and secondary visual cortices V1 and V2 were detected in 10 ICs (ICs 1, 2, 4, 21, 32, 38, 52, 59, 61, and 63), and the largest overlap for V1 was in ICs 21 and 55, both having 55.5%. The secondary V2 had the largest overlaps in ICs 21 (51%) and IC 59 (54%). The multiple components have a strong resemblance to natural viewing (V1–V5, lateral occipital complexes) and listening-related components in the occipital and temporal regions [Bartels and Zeki, 2005; Malinen et al., 2007]. The positive/negative ICs 52 and 61 resemble visual fields seen in visual hemifield activation study using the frequency based group ICA [Calhoun et al., 2003].

IC 25 was the one most overlapping with the primary auditory cortex (90.5% with the right TE 1.0 and 89.7% with TE 1.2 on the left) and is left-dominant. The primary auditory cortex was connected to 10 ICs (ICs 1, 15, 18, 25, 29, 37, 39, 43, 47, 68). Broca's area had connectivity with 16 sources (ICs 3, 4, 7, 8, 9, 10, 15, 30, 31, 35, 37, 39, 43, 49, 66, 68) with largest nodes in IC 30 (77% right side), IC 35 (97% left side). Several other frontal and temporal sources have interesting and complex connectivity with various functional regions related to attention, language, and other cognitive functions. Their spatial overlapping with presently known anatomical regions are rich, just like those of the primary sensory and motor cortices, and they are presented more precisely in the Supporting Information Table I.2.

Recent findings show that the DMN nodes have separate causality and connectivity characteristics [Sridharan et al., 2008; Uddin et al., 2009]. Also researchers using ICA have noticed the separation of the DMN into at least two subnetworks [Calhoun et al., 2008; Damoiseaux et al., 2006]. The results of this study show that the DMN is functionally differentiated into anterior and posterior parts. There are also "DMN-type" components (ICs 7, 10, 23, 18, and 37) with clear spatial overlap with DMN related areas [Buckner et al., 2008]. The detection of these areas is particularly sensitive to model order of the ICA and we are currently investigating this phenomenon.

The regions detected as anticorrelated with the DMN in correlation analyses using global mean regression were also detected as sources of their own (ICs 6, 40, 49). The use of ICA avoids the problematic regression of the global mean signal, although the PCA mean subtraction step in preprocessing of PICA also alters the data to some extent [Murphy et al., 2009]. On the basis of the present results, the areas anticorrelated to DMN in correlation analyses are also present as independent signal sources and therefore may not be completely a by-product of global mean signal regression of BOLD signal.

To maximize the chances of effective treatment, it is crucially important to identify diseases at the earliest stage possible. Functional alterations often present themselves as symptoms prior to irreversible tissue damage. For clinical brain research, function-based tissue segmentation is of pivotal importance in the early detection and characterization of diseases. Greicius et al. [2004, 2007] have already shown that minimally impaired memory deficiency or depression are related to the function of a brain network. ICA analyses detecting multiple brain networks have shown that, while some networks show no changes, others may be more affected by diseases such as Alzheimer's and schizophrenia [Calhoun et al., 2008; Jafri et al., 2008; Sorg et al., 2007]. The high model order ICA segmentation increases functional and anatomical specificity in the connectivity analysis of the networks and so may enhance our ability to detect disease-related network alterations.

The ICA methodology in this study is widely used by other researchers, and we suggest that the relatively high number of detected RSN components is due to increased signal-to-noise ratio related to the large dataset used in the group analysis. How inter-subject variance affects the results is, however, an important question; are we seeing more fringe components that are only present on subpopulations within the group [Schmidhorst and Holland, 2004]? For example, bored, anxious, or enthusiastic subjects might have different strengths of fluctuations in default mode subnetworks. The answer to this problem is also related to model order of a large group dataset and therefore this issue may not be entirely handled within the scope of this manuscript.

The only minor alteration compared to general trends in ICA analyses was the utilization of 70 components. The high model order is supported by the works of McKeown et al. [2002] and some recent ones as well [De Martino et al., 2007; Malinen et al., 2007]. One can always speculate on the effects of over-fitting in the detected components, if there are any. It should be noted that model order estimation with PPCA also yielded high model order numbers, i.e. 73 in this dataset, which strongly speaks against major overfitting. Two of the original 73 components were related to nonaccurate extra brain tissue removal, and this was corrected by utilizing another bet-algorithm outside the MELODICA automated tool.

To validate the stability of the method, we employed ICASSO on the pre-processed MELODIC data matrix. In doing so, 60 of the 70 components were shown to have a stability value of at least 0.7 in the group analysis, especially when the ICASSO was computed using a low epsilon threshold. Higher epsilon thresholds led to less clustered components in repeated runs due to less demanding convergence of the ICA algorithm around local maxima. It should be interesting to see how the repeated

**TABLE 1. Overlap with FSL templates, maximum t-score MNI-coordinates & clustering index of group-PICA RSN-sources**

| No. of IC | Anatomical ROI area | Area | Overlap % | *t*-score | | MNI max-*t* | | | Template | No. of ICASSO | Spatial correlation | $I_q$ |
|---|---|---|---|---|---|---|---|---|---|---|---|---|
| | | | IC vs. ROI | Mean | Max | *X* | *Y* | *Z* | Source | | | |
| 1 | GM Visual cortex V5 | R/L | 60.0/55.0 | 6.7/5.6 | 14.0/11.0 | 27/67 | 31/26 | 28/31 | J | 15 | 0.86 | 0.964 |
| | Temporal Occipital Fusiform Cortex | | 66.5 | 7.3 | 20.1 | 30 | 29 | 26 | HO | | | |
| | Occipital Fusiform Gyrus | | 78.0 | 8.1 | 20.6 | 30 | 28 | 26 | HO | | | |
| | Lateral Occipital Cortex, inferior division | | 58.0 | 6.7 | 20.1 | 30 | 27 | 26 | HO | | | |
| 2 | GM Visual cortex V1 BA17 | V1/V2 | 37.0/37.5 | 8.5/8.6 | 31.3/31.3 | 60/60 | 16/16 | 34/34 | J | 63 | 0.84 | 0.810 |
| | GM Visual cortex V2 BA18 | | 37.5 | 8.6 | 31.3 | 60 | 16 | 34 | J | | | |
| | Occipital Fusiform Gyrus | | 55.0 | 4.9 | 31.3 | 60 | 16 | 34 | HO | | | |
| 3 | GM Premotor cortex BA6 | R/L | 30.0/31.0 | 5.8/6.0 | 13.8/13.5 | 32/54 | 74/74 | 66/66 | J | | | |
| | Superior Frontal Gyrus | | 43.6 | 6.9 | 14.6 | 30 | 74 | 64 | HO | | | |
| | Middle Frontal Gyrus | | 42.0 | 6.8 | 14.6 | 30 | 74 | 64 | HO | | | |
| 4 | GM Visual cortex V5 | R/L | 73.0/62.0 | 5.9/5.4 | 11.2/9.9 | 24/64 | 22/21 | 42/41 | J | 61 | 0.56 | 0.627 |
| | Lateral Occipital Cortex, superior division | | 44.9 | 6.8 | 17.0 | 52 | 18 | 52 | HO | | | |
| | Cuneal Cortex | | 55.8 | 6.8 | 17.0 | 52 | 18 | 52 | HO | | | |
| 6 | GM Anterior intra-parietal sulcus hIP2 | R/L | 78.0/56.0 | 7.5/5.2 | 18.2/12.0 | 13/76 | 50/48 | 52/50 | J | 43 | 0.83 | 0.821 |
| | GM Secondary somatosensory cortex/Parietal operculum OP1 | | 61.5 | 9.0 | 19.0 | 12 | 52 | 54 | J | | | |
| | Supramarginal Gyrus, anterior division | | 68.8 | 7.3 | 19.0 | 12 | 52 | 54 | HO | | | |
| 7 | GM Anterior intra-parietal sulcus hIP1 | | 32.9 | 6.7 | 17.0 | 70 | 32 | 50 | J | 46 | 0.84 | 0.730 |
| | GM Visual cortex V5 | | 46.3 | 5.0 | 14.4 | 71 | 29 | 48 | J | | | |
| | Middle Temporal Gyrus, temporooccipital part | | 38.8 | 5.2 | 16.4 | 73 | 32 | 48 | HO | | | |
| | Angular Gyrus | | 36.2 | 6.5 | 18.0 | 72 | 32 | 50 | | | | |
| 8 | Frontal Pole | | 27.2 | 6.8 | 21.3 | 44 | 94 | 46 | HO | 9 | 0.90 | 0.950 |
| | Superior Frontal Gyrus | | 27.8 | 7.0 | 21.0 | 44 | 94 | 47 | HO | | | |
| | Paracingulate Gyrus | | 28.6 | 6.3 | 18.8 | 43 | 92 | 48 | HO | | | |
| 9 | GM Anterior intra-parietal sulcus hIP1 | | 68.9 | 6.4 | 15.5 | 30 | 28 | 60 | J | 26 | 0.86 | 0.914 |
| | GM Anterior intra-parietal sulcus hIP2 | | 56.7 | 5.0 | 10.2 | 24 | 36 | 62 | J | | | |
| | Lateral Occipital Cortex, superior division | | 32.6 | 6.2 | 17.5 | 32 | 26 | 62 | HO | | | |
| 10 | GM Broca's area BA45 | | 20.6 | −1.9 | 4.1 | 24 | 82 | 36 | J | 4 | 0.72 | 0.982 |
| | WM Cingulum | | 20.0 | 3.0 | 9.0 | 50 | 85 | 36 | J | | | |
| | Frontal Medial Cortex | | 65.3 | 8.7 | 22.2 | 46 | 92 | 32 | HO | | | |
| | Paracingulate Gyrus | | 50.5 | 6.5 | 22.2 | 46 | 92 | 32 | HO | | | |

**TABLE I. (continued)**

| No. of IC | Anatomical ROI area | Area | Overlap % IC vs. ROI | *t*-score Mean | *t*-score Max | MNI max-*t* *X* | MNI max-*t* *Y* | MNI max-*t* *Z* | Template Source | No. of ICASSO | Spatial correlation | $I_q$ |
|---|---|---|---|---|---|---|---|---|---|---|---|---|
| 13 | GM Amygdala_laterobasal group | R/L | 37.0/37.0 | 5.6/5.1 | 11.0/9.5 | 27/67 | 63/68 | 17/20 | J | 8 | 0.94 | 0.947 |
| | GM Hippocampus entorhinal cortex | R/L | 40.0/38.0 | 5.5/4.8 | 11.5/10.0 | 27/62 | 63/60 | 16/16 | J | | | |
| | Inferior Temporal Gyrus, anterior division | | 76.7 | 7.8 | 14.5 | 68 | 68 | 16 | HO | | | |
| | Temporal Fusiform Cortex, anterior division | | 73.8 | 6.8 | 13.6 | 22 | 64 | 16 | HO | | | |
| 14 | GM Primary somatosensory cortex BA3a | R/L | 19.8/33.6 | 5.0/5.5 | 10.8/12.8 | 42/51 | 41/44 | 62/60 | J | 11 | 0.78 | 0.939 |
| | Cingulate Gyrus, posterior division | | 40.7 | 6.6 | 12.9 | 50 | 44 | 60 | HO | | | |
| | Precuneous Cortex | | 40.2 | 5.7 | 12.9 | 50 | 44 | 60 | HO | | | |
| | Cuneal Cortex | | 21.4 | 3.9 | 6.4 | 38 | 32 | 58 | HO | | | |
| 15 | GM Broca's area BA44 | R/L | 44.9/30.7 | 4.2/4.5 | 13.0/14.6 | 18/67 | 74/75 | 34/32 | J | 67 | 0.84 | 0.579 |
| | GM Broca's area BA45 | R/L | 53.1/45.5 | 5.0/5.3 | 13.5/15.1 | 19/68 | 74/74 | 32/32 | J | | | |
| | Inferior Frontal Gyrus, | pars tria./operc. | 51.0/42.6 | 5.5/5.3 | 15.1/14.6 | 68/69 | 74/74 | 32/32 | HO | | | |
| | Paracingulate Gyrus | | 43.2 | 3.9 | 8.2 | 46 | 74 | 60 | HO | | | |
| | Frontal Operculum Cortex | | 66.4 | 7.6 | 15.1 | 68 | 74 | 32 | HO | | | |
| 18 | GM Primary auditory cortex TE1.1 | R/L | 44.0/64.0 | 3.3/4.1 | 4.9/6.3 | 24/66 | 48/50 | 44/40 | J | 60 | 0.72 | 0.746 |
| | Paracingulate Gyrus | | 62.7 | 6.4 | 19.0 | 44 | 76 | 48 | HO | | | |
| | Cingulate Gyrus, anterior division | | 68.5 | 7.0 | 19.0 | 44 | 76 | 48 | HO | | | |
| 19 | GM Primary motor cortex BA4a(+p) | R/L | 50.2/50.8 | 7.4/8.0 | 15.3/15.4 | 45/46 | 52/52 | 68/68 | J | 35 | 0.90 | 0.919 |
| | GM Primary somatosensory cortex BA3a(+1-3b) | R | 41.0/39.8 | 7.8/7.7 | 14.6/15.0 | 44/56 | 50/48 | 66/66 | J | | | |
| | Juxtapositional Lobule Cortex | | 35.6 | 7.2 | 15.4 | 46 | 52 | 68 | HO | | | |
| 21 | GM Visual cortex V1 BA17 | V1/V2 | 55.5/51.2 | 8.7/7.7 | 26.8/26.8 | 42/42 | 18/18 | 36/36 | J | 66 | 0.91 | 0.645 |
| | Intracalcarine Cortex | | 51.5 | 10.3 | 26.8 | 42 | 18 | 36 | HO | | | |
| | Occipital Pole | | 52.3 | 8.3 | 26.8 | 42 | 18 | 36 | HO | | | |
| 23 | GM Anterior intra-parietal sulcus hIP1-2 | R/L | 47.5/38.1 | 8.0/5.6 | 19.0/12.5 | 20/69 | 34/34 | 59/60 | J | 30 | 0.81 | 0.859 |
| | Supramarginal Gyrus, posterior division | | 35.2 | 6.8 | 19.8 | 18 | 36 | 58 | HO | | | |
| | Angular Gyrus | | 50.4 | 7.8 | 19.8 | 18 | 36 | 58 | HO | | | |
| | Lateral Occipital Cortex, superoir division | | 29.3 | 5.7 | 19.8 | 18 | 36 | 58 | HO | | | |

**TABLE 1. (continued)**

| No. of IC | Anatomical ROI area | Area | Overlap % IC vs. ROI | *t*-score Mean | *t*-score Max | MNI max-*t* *X* | MNI max-*t* *Y* | MNI max-*t* *Z* | Template Source | No. of ICASSO | Spatial correlation | $I_q$ |
|---|---|---|---|---|---|---|---|---|---|---|---|---|
| 24 | GM Primary motor cortex BA4a+p | R/L | 38.6/35.8 | 7.0/5.8 | 12.7/13.5 | 40/50 | 56/57 | 74/74 | J | 58 | 0.67 | 0.907 |
| | GM Primary somatosensory cortex BA1 | R/L | 34.4/31.1 | 6.4/4.7 | 12.1/11.6 | 30/50 | 50/51 | 72/74 | J | | | |
| | GM Premotor cortex BA6 R | R/L | 27.0/27.5 | 6.6/5.8 | 12.7/13.6 | 40/52 | 56/58 | 74/74 | J | | | |
| | Juxtapositional Lobule Cortex (SMA) | | 26.0 | 4.7 | 13.5 | 50 | 58 | 74 | HO | | | |
| 25 | GM Primary auditory cortex TE1.0 (-1.2) | R/L | 90.5/87.6 | 8.1/8.9 | 17.7/19.3 | 14/76 | 52/50 | 40/40 | J | 14 | 0.94 | 0.925 |
| | GM Secondary somatosensory cortex/Parietal operculum OP1 | R/L | 39.7/52.9 | 6.7/9.2 | 17.0/19.3 | 14/76 | 53/50 | 40/40 | J | | | |
| | Heschl's Gyrus (includes H1 and H2) | | 90.6 | 8.7 | 19.4 | 76 | 50 | 40 | HO | | | |
| 27 | GM Anterior intra-parietal sulcus hIP2 | R/L | 49.3/48.9 | 7.0/7.9 | 17.9/18.7 | 22/70 | 50/48 | 63/61 | J | 69 | 0.88 | 0.578 |
| | GM Primary motor cortex BA4p (+a) | | 35.3 | 7.9 | 18.3 | 22 | 51 | 64 | J | | | |
| | GM Primary somatosensory cortex BA2 | R/L | 55.6/59.8 | 7.6/9.9 | 18.3/19.8 | 22/66 | 52/52 | 64/66 | J | | | |
| | Supramarginal Gyrus, anterior division | | 56.3 | 6.4 | 19.3 | 68 | 48 | 63 | HO | | | |
| 29 | GM Amygdala_centromedial group | R/L | 68.6/40.1 | 5.0/4.5 | 11.6/9.6 | 24/62 | 61/54 | 26/31 | J | 23 | 0.90 | 0.940 |
| | GM Hippocampus cornu ammonis | R/L | 41.0/32.6 | 5.2/5.3 | 12.9/13.7 | 24/65 | 57/54 | 29/30 | J | | | |
| | GM Lateral geniculate body | R/L | 54.4/42.7 | 3.5/3.4 | 5.8/5.7 | 30/60 | 55/53 | 32/30 | J | | | |
| | Planum Polare | | 64.5 | 7.7 | 15.6 | 66 | 56 | 30 | HO | | | |
| 30 | GM Anterior intra-parietal sulcus hIP1 | R/L | 37.9/21.6 | 3.8/3.7 | 6.2/5.8 | 26/24 | 34/36 | 60/60 | J | 33 | 0.84 | 0.923 |
| | GM Broca's area BA44 (+BA45) | R/L | 77.5/33.9 | 6.7/4.4 | 13.1/8.3 | 20/68 | 70/72 | 48/48 | J | | | |
| | GM Secondary somatosensory cortex/Parietal operculum OP3 (+OP2,4) | R | 55.3 | 4.5 | 10.5 | 22 | 65 | 46 | J | | | |
| | Inferior Frontal Gyrus, pars opercularis | | 63.9 | 6.3 | 13.1 | 20 | 70 | 48 | HO | | | |
| | Right Caudate | | 20.0 | 3.1 | 4.2 | 34 | 61 | 46 | HO | | | |
| 31 | GM Broca's area BA45 | R/L | 16.7/29.0 | 0.4/4.0 | 7.4/11.1 | 22/66 | 86/86 | 45/43 | | 54 | 0.69 | 0.665 |
| | Frontal Pole | | 42.5 | 5.1 | 18.6 | 60 | 94 | 40 | | | | |
| | Inferior Frontal Gyrus, pars triangularis | | 22.3 | 1.5 | 8.8 | 66 | 84 | 45 | | | | |

**TABLE I. (continued)**

| No. of IC | Anatomical ROI area | Area | Overlap % IC vs. ROI | *t*-score Mean | *t*-score Max | MNI max-*t* *X* | MNI max-*t* *Y* | MNI max-*t* *Z* | Template Source | No. of ICASSO | Spatial correlation | $I_q$ |
|---|---|---|---|---|---|---|---|---|---|---|---|---|
| 32 | GM Hippocampus subiculum | R/L | 42.9/48.2 | 4.8/5.4 | 9.4/11.02 | 32/58 | 42/43 | 30/30 | J | 28 | 0.66 | 0.936 |
| | GM Visual cortex V2 BA18 | | 26.0 | 3.4 | 9.9 | 52 | 34 | 38 | J | | | |
| | GM Medial (+lateral) geniculate body | R/L | 55.8/88.5 | 3.4/3.9 | 4.9/6.2 | 38/50 | 47/46 | 29/30 | J | | | |
| | Parahippocampal Gyrus, posterior division | | 83.3 | 5.7 | 12.0 | 58 | 42 | 28 | HO | | | |
| 34 | Cerebellum | | | | | | | | | 13 | 0.91 | 0.935 |
| 35 | GM Broca's area BA45(+BA45) | R/L | 19.4/97.0 | 3.5/8.8 | 5.6/17.7 | 20/70 | 80/84 | 40/36 | J | 42 | 0.84 | 0.811 |
| | Inferior Frontal Gyrus, pars triangularis | | 59.6 | 8.0 | 17.7 | 70 | 84 | 36 | J | | | |
| | Inferior Frontal Gyrus, pars opercularis | | 51.5 | 6.7 | 16.5 | 70 | 78 | 41 | J | | | |
| | Frontal Operculum Cortex | | 39.7 | 5.8 | 15.6 | 70 | 77 | 41 | J | | | |
| 37 | Frontal Pole | | 32.2 | 4.5 | 15.7 | 28 | 84 | 54 | HO | 34 | 0.69 | 0.897 |
| | Superior Frontal Gyrus | | 27.5 | 3.9 | 15.7 | 28 | 84 | 54 | HO | | | |
| | Middle Frontal Gyrus | | 36.9 | 5.5 | 15.7 | 28 | 84 | 54 | HO | | | |
| | Paracingulate Gyrus | | 22.9 | 1.0 | 5.1 | 41 | 90 | 53 | HO | | | |
| 38 | Cingulate Gyrus, posterior division | | 50.5 | 8.2 | 19.7 | 46 | 33 | 50 | HO | 65 | 0.83 | 0.883 |
| | Precuneous Cortex | | 43.8 | 8.0 | 19.9 | 46 | 32 | 50 | HO | | | |
| | Cuneal Cortex | | 40.2 | 8.4 | 19.7 | 46 | 31 | 50 | HO | | | |
| | Supracalcarine Cortex | | 53.6 | 9.2 | 19.9 | 46 | 32 | 50 | HO | | | |
| 39 | GM Visual cortex V5 | R/L | 91.5/56.0 | 7.1/4.0 | 12.7/6.2 | 18/70 | 34/32 | 38/36 | J | 16 | 0.86 | 0.923 |
| | Middle Temporal Gyrus, temporooccipital part | | 69.4 | 6.4 | 14.6 | 20 | 38 | 38 | J | | | |
| | Inferior Temporal Gyrus, temporooccipital part | | 37.7 | 5.9 | 13.3 | 17 | 37 | 36 | J | | | |
| | Lateral Occipital Cortex, inferior division | | 34.2 | 5.3 | 13.6 | 20 | 36 | 38 | J | | | |
| 40 | GM Primary somatosensory cortex BA2 | R/L | 36.8/39.0 | 5.6/6.4 | 15.0/12.7 | 32/58 | 36/36 | 70/70 | J | 20 | 0.82 | 0.908 |
| | Postcentral Gyrus | | 22.1 | 5.2 | 14.9 | 33 | 36 | 70 | HO | | | |
| | Superior Parietal Lobule | | 52.1 | 6.1 | 15.0 | 32 | 36 | 70 | HO | | | |
| | Lateral Occipital Cortex, superoir division | | 20.3 | 5.6 | 15.0 | 32 | 36 | 70 | HO | | | |
| | Precuneous Cortex | | 17.8 | 3.4 | 13.7 | 37 | 34 | 70 | HO | | | |
| 41 | GM Amygdala_centromedial group | R/L | 80.1/76.3 | 6.9/6.2 | 18.4/14.6 | 31/58 | 64/63 | 32/32 | J | 12 | 0.93 | 0.942 |
| | Putamen | R/L | 92.7/93.4 | 9.4/7.9 | 21.0/18.4 | 58/32 | 66/66 | 34/32 | HO | | | |
| | Pallidum | | 80.0/80.4 | 5.5/7.0 | 11.4/16.9 | 56/54 | 66/70 | 34/33 | HO | | | |
| | Accumbens | R/L | 51.4/55.7 | 5.4/5.5 | 12.3/11.4 | 36/54 | 70/70 | 32/33 | HO | | | |

**TABLE 1. (continued)**

| No. of IC | Anatomical ROI area | Area | Overlap % IC vs. ROI | *t*-score Mean | *t*-score Max | MNI max-*t* *X* | MNI max-*t* *Y* | MNI max-*t* *Z* | Template Source | No. of ICASSO | Spatial correlation | $I_q$ |
|---|---|---|---|---|---|---|---|---|---|---|---|---|
| 43 | GM Primary auditory cortex TE1.2 | R/L | 59.9/43.5 | 9.9/8.7 | 26.2/23.5 | 14/74 | 60/58 | 43/45 | J | 1 | 0.95 | 0.984 |
| | GM Primary somatosensory cortex BA3b | R/L | 37.2/37.2 | 14.0/13.4 | 34.1/33.7 | 16/72 | 60/58 | 48/50 | J | | | |
| | GM Secondary somatosensory cortex/Parietal operculum OP4 (OP1-3) | R/L | 72.9/71.9 | 12.2/12.3 | 34.1/33.7 | 16/72 | 60/58 | 48/50 | J | | | |
| | Central Opercular Cortex | | 39.3 | 10.0 | 30.7 | 16 | 60 | 46 | HO | | | |
| 45 | GM Medial geniculate body | R/L | 24.7/16.4 | 3.0/3.0 | 3.5/3.5 | 38/49 | 52/48 | 33/30 | J | 17 | 0.90 | 0.901 |
| | Brain-Stem | | 22.3 | 4.2 | 11.1 | 42 | 40 | 24 | HO | | | |
| | Right Thalamus | | 8.5 | 3.3 | 4.3 | 40 | 52 | 34 | HO | | | |
| 47 | GM Primary auditory cortex TE1.2 | R/L | 31.2/43.7 | 4.5/4.5 | 7.9/7.8 | 22 | 60 | 36 | J | 47 | 0.82 | 0.795 |
| | Subcallosal Cortex | | 29.0 | 6.6 | 16.4 | 44 | 78 | 38 | HO | | | |
| | Paracingulate Gyrus | | 31.7 | 5.7 | 16.4 | 44 | 81 | 38 | HO | | | |
| | Cingulate Gyrus, anterior division | | 33.8 | 6.8 | 17.1 | 44 | 80 | 38 | HO | | | |
| | Left Accumbens | | 31.4 | 4.4 | 8.6 | 48 | 74 | 36 | HO | | | |
| 49 | GM Broca's area BA44 | R/L | 53.5/41.1 | 5.3/1.8 | 12.9/10.2 | 16/74 | 66/64 | 36/36 | J | 57 | 0.65 | 0.586 |
| | GM Primary auditory cortex TE1.2 | R/L | 99.8/91.0 | 7.6/5.6 | 13.0/10.2 | 16/74 | 66/64 | 36/36 | J | | | |
| | Insular Cortex | | 59.7 | 5.4 | 12.7 | 24 | 66 | 36 | J | | | |
| | Juxtapositional Lobule Cortex (SMA) | | 57.9 | 4.9 | 11.4 | 44 | 66 | 58 | HO | | | |
| | Frontal Operculum Cortex | | 62.0 | 6.0 | 13.0 | 16 | 66 | 36 | HO | | | |
| | Central Opercular Cortex | | 65.2 | 6.1 | 13.0 | 16 | 66 | 36 | HO | | | |
| | Planum Polare | | 69.8 | 6.3 | 13.0 | 16 | 66 | 36 | HO | | | |
| 52 | GM Visual cortex V1 BA17 | L, V1/V2 | 19.7/19.4 | 1.7/1.6 | 16.6/15.8 | 54/52 | 18/18 | 24/25 | J | 32 | 0.73 | 0.888 |
| | Lateral Occipital Cortex, inferior division | L | 24.5 | 3.6 | 17.1 | 56 | 20 | 24 | J | | | |
| | Occipital Fusiform Gyrus | L | 34.7 | 5.9 | 17.1 | 56 | 20 | 24 | HO | | | |
| | Occipital Pole | L | 28.1 | 1.7 | 17.0 | 52 | 18 | 24 | HO | | | |
| 53 | GM Primary motor cortex BA4a | L | 18.9 | 4.5 | 10.5 | 60 | 58 | 62 | J | 41 | 0.30 | 0.942 |
| | Superior Frontal Gyrus | | 19.7 | 5.5 | 12.2 | 58 | 60 | 64 | HO | | | |
| | Middle Frontal Gyrus | | 14.2 | 5.5 | 12.2 | 58 | 60 | 64 | HO | | | |
| | Juxtapositional Lobule Cortex (SMA) | | 25.8 | 4.1 | 7.9 | 53 | 64 | 64 | HO | | | |
| 59 | GM Visual cortex V1 BA17 | | 55.5 | 9.7 | 22.3 | 50 | 28 | 38 | J | 10 | 0.88 | 0.951 |
| | GM Visual cortex V2 BA18 | R | 54.4 | 9.3 | 22.3 | 50 | 28 | 38 | J | | | |
| | Intracalcarine Cortex | R | 86.9 | 12.0 | 22.3 | 50 | 28 | 38 | HO | | | |
| | Lingual Gyrus | R | 63.1 | 10.4 | 22.3 | 50 | 28 | 38 | HO | | | |
| | Supracalcarine Cortex | R | 68.6 | 11.6 | 22.3 | 50 | 28 | 38 | HO | | | |

**TABLE I. (continued)**

| No. of IC | Anatomical ROI area | Area | Overlap % | *t*-score | | MNI max-*t* | | | Template | No. of ICASSO | Spatial correlation | $I_q$ |
|---|---|---|---|---|---|---|---|---|---|---|---|---|
| | | | IC vs. ROI | Mean | Max | *X* | *Y* | *Z* | Source | | | |
| 60 | GM Anterior intra-parietal sulcus hIP2 | R | 49.4 | 4.4 | 8.4 | 25 | 51 | 62 | J | 52 | 0.79 | 0.678 |
| | GM Primary motor cortex BA4p | R | 47.9 | 5.5 | 11.0 | 33 | 56 | 64 | J | | | |
| | GM Primary somatosensory cortex BA2 | R | 50.0 | 4.6 | 9.1 | 24 | 53 | 64 | J | | | |
| | GM Premotor cortex BA6 | R | 55.1 | 6.1 | 13.8 | 32 | 60 | 64 | J | | | |
| 61 | GM Visual cortex V1 BA17 | R | 23.8 | 2.8 | 16.5 | 36 | 18 | 26 | J | 55 | 0.64 | 0.627 |
| | GM Visual cortex V2 BA18 | | 22.4 | 2.7 | 16.6 | 32 | 20 | 26 | J | | | |
| | Occipital Fusiform Gyrus | | 33.7 | 5.8 | 16.7 | 32 | 20 | 24 | HO | | | |
| | Occipital Pole | | 32.0 | 3.9 | 16.6 | 32 | 20 | 25 | HO | | | |
| 63 | Lateral Occipital Cortex, superior division | | 21.3 | 6.0 | 25.0 | 43 | 24 | 58 | J | 61 | 0.61 | 0.628 |
| | Precuneous Cortex | | 30.9 | 8.1 | 25.1 | 44 | 24 | 56 | J | | | |
| | Cuneal Cortex | | 54.0 | 8.9 | 25.1 | 44 | 24 | 56 | J | | | |
| | Supracalcarine Cortex | | 29.7 | 6.7 | 23.2 | 42 | 25 | 56 | J | | | |
| 66 | Frontal Medial Cortex | | 33.9 | 6.6 | 15.2 | 42 | 94 | 28 | | 4 | 0.70 | 0.971 |
| | Juxtapositional Lobule Cortex (SMA) | | 25.7 | 3.4 | 5.2 | 48 | 64 | 58 | | | | |
| | Middle Temporal Gyrus, temporooccipital part | | 19.6 | 3.6 | 6.0 | 72 | 36 | 40 | | | | |
| 68 | GM Broca's area BA44 | | 20.7 | 4.6 | 24.5 | 29 | 68 | 56 | J | 68 | 0.70 | 0.602 |
| | GM Primary auditory cortex TE1.2 | | 24.4 | 3.1 | 74.7 | 78 | 53 | 42 | J | | | |
| | GM Visual cortex V5 | | 33.2 | 3.6 | 19.2 | 20 | 28 | 47 | J | | | |
| | Superior Frontal Gyrus | | 21.8 | 5.6 | 33.6 | 32 | 70 | 56 | HO | | | |
| | | | | | | | | | | max | 0.95 | 0.984 |
| | | | | | | | | | | mean | 0.79 | 0.829 |
| | | | | | | | | | | std | 0.13 | 0.132 |

No. of IC = number of selected component, Anatomical ROI Area = Name of anatomical template from fsl4, Area = side or other anatomical specification R = right, L= left, Overlap % = anatomical overlap percentage of components vs. anatomical structure, *t*-score = *t*-value (mean, maximum [Max]), MNI max-*t* = maximum *t*-value X, Y & Z-direction Montreal Neurologic Institute 152 coordinates, Template source = anatomical ROI source in fsl4: J = Juelich, HO = Harvard-Oxford template, # ICASSO = icasso run equivalent to selected IC, spatial correlation = spatial correlation between ICASSO and selected IC, Iq = ICASSO clustering index.

ICASSO analysis results differentiate from single subject run PICA results. We are currently exploring the benefits of using both PICA and ICASSO in a combined analysis setting. Another unclear issue is how the RSN's detected in the group data can be used in individual settings. On the basis of the results shown here, a familiar ICA-related issue reemerges; what is the optimal model order of ICA in datasets with increased subject numbers, and how are preprocessing schemes influencing the results? We are currently investigating whether it is still possible to detect more accurate RSN components with bigger data samples and higher model orders.

The temporal correlation matrix of the ICA enables the assessment of connectivity between all the detected signal sources. It can be seen that some of the sources have limited correlation to practically all the other sources, which becomes visible as a dark row in the mean connectivity matrix (c.f. Fig. 5). These dark lines tend to be non-RSNs sources related to noise/artifacts and, indeed, their mean *temporal* intersource connectivity is significantly lower than those of the RSN sources. The temporal correlation structure could perhaps be used as a feature in differentiating the non-RSN and RSN sources with different lag periods. The non-RSN sources are thus temporally more *independent* than the connected RSN sources, and therefore their automated separation seems feasible from this point of view [De Martino et al., 2007; Tohka et al., 2008].

There have been concerns about the uncontrolled nature of the resting state regarding attention and free thinking induced alterations. In this study, we used a semi-resting state by instructing the subject to fixate on a cross shown on the screen. The subject is not completely at rest and tries to sustain attention on the cross. On the other hand, no restrictions on the fixation or mental imagery were given either. The fixation reduces motion artifacts and still offers some cognitive baseline function to reduce some of the variability of free thinking. McAvoy et al. [2008] recently presented rather similar spatial distribution of areas where BOLD fluctuation frequency is dependent on whether the subject has eyes open, closed, or is fixating on a cross. We found a similar distribution of areas, and in addition differences in power spectral densities between the visual area sources. The V1-related medial (IC 59) and dorsal (IC 21) components in this study have somewhat different rank-1 approximates from the other occipital sources. It would be interesting to see how these sources differ in subjects with eyes closed in a large number of subjects.

Importantly, it has been shown that the effective estimation and removal of underlying oscillations significantly improves the signal-to-noise ratio in the task activation studies [Fox et al., 2006]. In addition, baseline activity oscillations preceding stimuli explains the major share of the subsequent stimulus response variability [Boly et al., 2007; Fox et al., 2006; Eichele et al., 2008]. There may be stimulus-locked connectivity alterations that can be masked by the baseline oscillations, rendering the hemodynamic response functions and correlation-based connectivity measurement inaccurate. After establishing the cortical oscillatory activity within each of the networks with high model order ICA, one may be able to utilize these baseline oscillations in a regression analysis in a more accurate manner, and obtain increased signal-to-noise ratios in stimulus related effective connectivity analyses of brain networks. Also, due to the fact that ICA separates noise sources, the mixing matrix signals seem to yield effective measures for connectivity and causality measurements, without biasing physiological or motion related correlations [Calhoun et al., 2008; Eichele et al., 2008; Sorg et al., 2007].

Mantini et al. [2007] were able to distinguish EEG power distribution fingerprints of different RSNs. Although the frequency resolution of fMRI alone is not as good as that of EEG, one is able to depict differences between the power distributions and first rank approximates of the RSNs (c.f. Figs. 2–4). Primary sensory and motor sources, default mode, Broca's area, and some occipital visual sources present some prominent frequency peaks in addition to the $1/f$ trend in the spectrum. The frontal sources predominantly have $1/f$ distributions without clear peaks. The functional significance of this difference in peak frequency distributions needs further elucidation.

## CONCLUSION

The brain cortex can be robustly segmented into 42 independent RSNs by utilizing the group-ICA of baseline BOLD data. This method offers complementary information on tissue characteristics of cortical structures compared to previous post-mortem histological and microanatomic dissection of structures. Utilization of a relatively high model order and multi-subject group data enables increased accuracy of functional segmentation of brain tissue due to increased signal-to-noise ratio. The method reveals multiple interlinked connectivity subnetworks enabling more fine-tuned characterization of seed regions for further causality and connectivity analyses.

## ACKNOWLEDGMENTS

The authors cordially thank Dr. Christian Beckmann for his assistance in PICA mixing matrix and bet analyses, and, Dr Gordon Roberts for editorial assistance. The authors would also like to express their deep gratitude to the reviewers and handling editor for their excellent suggestions and corrections on the manuscript. This study was supported by Academy of Finland Grant #111711, Finnish Medical Foundation and Finnish Neurological Association grants.

## REFERENCES

Bartels A, Zeki S (2005): The chronoarchitecture of the cerebral cortex. Philos Trans R Soc Lond B Biol Sci 360:733–750.

Beckmann CF, Smith SM (2004): Probabilistic independent component analysis for functional magnetic resonance imaging. IEEE Trans Med Imaging 23:137–152.

Beckmann CF, DeLuca M, Devlin JT, Smith SM (2005): Investigations into resting-state connectivity using independent component analysis. Philos Trans R Soc Lond B Biol Sci 360:1001–1013.

Biswal BB, Yetkin FZ, Haughton VM, Hyde JS (1995): Functional connectivity in the motor cortex of resting human brain using echo-planar MRI. Magn Reson Med 34:537–541.

Birn RM, Diamond JB, Smith MA, Bandettini PA. (2006): Separating respiratory-variation-related fluctuations from neuronal-activity-related fluctuations in fMRI. Neuroimage 31:1536–1548.

Boly M, Balteau E, Schnakers C, Degueldre C, Moonen G, Luxen A, Phillips C, Peigneux P, Maquet P, Laureys S (2007): Baseline brain activity fluctuations predict somatosensory perception in humans. Proc Natl Acad Sci USA 104:12187–12192.

Calhoun VD, Adali T, Pearlson GD, Pekar JJ (2001): A method for making group inferences from functional MRI data using independent component analysis. Hum Brain Mapp 14:140–151.

Calhoun VD, Adali T, Pekar JJ, Pearlson GD (2003): Latency (in)sensitive ICA. Group independent component analysis of fMRI data in the temporal frequency domain. Neuroimage 20:1661–1669

Calhoun VD, Kiehl KA, Pearlson GD (2008): Modulation of temporally coherent brain networks estimated using ICA at rest and during cognitive tasks. Hum Brain Mapp 29:828–838.

Cohen AL, Fair DA, Dosenbach NU, Miezin FM, Dierker D, Van Essen DC, Schlaggar BL, Petersen SE (2008): Defining functional areas in individual human brains using resting functional connectivity MRI. NeuroImage 41:45–57.

Damoiseaux JS, Rombouts SA, Barkhof F, Scheltens P, Stam CJ, Smith SM, Beckmann CF (2006): Consistent resting-state networks across healthy subjects. Proc Natl Acad Sci USA 103:13848–13853.

De Martino F, Gentile F, Esposito F, Balsi M, Di Salle F, Goebel R, Formisano E (2007): Classification of fMRI independent components using IC-fingerprints and support vector machine classifiers. NeuroImage 34:177–194.

De Luca M, Beckmann CF, De Stefano N, Matthews PM, Smith SM (2006): fMRI resting state networks define distinct modes of long-distance interactions in the human brain. Neuroimage 29:1359–1367.

Di Martino A, Scheres A, Margulies DS, Kelly AM, Uddin LQ, Shehzad Z, Biswal B, Walters JR, Castellanos FX, Milham MP (2008): Functional connectivity of human striatum: A resting state fMRI study. Cereb Cortex 18:2735–2747.

Eichele T, Debener S, Calhoun VD, Specht K, Engel AK, Hugdahl K, von Cramon DY, Ullsperger M (2008): Prediction of human errors by maladaptive changes in event-related brain networks. Proc Natl Acad Sci 105:6173–6178.

Eickhoff SB, Paus T, Caspers S, Grosbras MH, Evans AC, Zilles K, Amunts K (2007): Assignment of functional activations to probabilistic cytoarchitectonic areas revisited. NeuroImage 36:511–521.

Fox MD, Raichle ME (2007): Spontaneous fluctuations in brain activity observed with functional magnetic resonance imaging. Nat Rev Neurosci 8:700–711.

Fox MD, Snyder AZ, Zacks JM, Raichle ME (2006): Coherent spontaneous activity accounts for trial-to-trial variability in human evoked brain responses. Nat Neurosci 9:23–25.

Fukunaga M, Horovitz SG, de Zwart JA, van Gelderen P, Balkin TJ, Braun AR, Duyn JH (2008): Metabolic origin of BOLD signal fluctuations in the absence of stimuli. J Cereb Blood Flow Metab 28:1377–1387.

Greicius MD, Srivastava G, Reiss AL, Menon V (2004): Default-mode network activity distinguishes Alzheimer's disease from healthy aging: Evidence from functional MRI. Proc Natl Acad Sci USA 101:4637–4642.

Greicius MD, Flores BH, Menon V, Glover GH, Solvason HB, Kenna H, Reiss AL, Schatzberg AF (2007): Resting-state functional connectivity in major depression: Abnormally increased contributions from subgenual cingulate cortex and thalamus. Biol Psychiatry 62:429–437.

Himberg J, Hyvärinen A, Esposito F (2004): Validating the independent components of neuroimaging time series via clustering and visualization. Neuroimage 22:1214–1222.

Hyvärinen A (1999): Fast and robust fixed-point algorithms for independent component analysis. IEEE Trans Neural Networks 10:626–634.

Jafri MJ, Pearlson GD, Stevens M, Calhoun VD (2008): A method for functional network connectivity among spatially independent resting-state components in schizophrenia. Neuroimage 39:1666–1681.

Jenkinson M, Bannister PR, Brady JM, Smith SM (2002): Improved optimisation for the robust and accurate linear registration and motion correction of brain images. NeuroImage 17:825–841.

Kannurpatti SS, Biswal BB, Kim YR, Rosen BR (2008): Spatio temporal characteristics of low frequency BOLD signal fluctuations in isoflurane anesthetized rat brain. NeuroImage 40:1738–1747.

Kenet T, Bibitchkov D, Tsodyks M, Grinvald A, Arieli A (2003): Spontaneously emerging cortical representations of visual attributes. Nature 425:954–956.

Kiviniemi V (2008): Endogenous brain fluctuations and diagnostic imaging. Hum Brain Mapp 29:810–817 (Review).

Kiviniemi V, Kantola J-H, Jauhiainen J, Hyvärinen A, Tervonen O (2003): Independent component analysis of non-deterministic fMRI signal sources. NeuroImage 19:253–260.

Li YO, Adali T, Calhoun VD (2007): Estimating the number of independent components for functional magnetic resonance imaging data. Hum Brain Mapp 11:1251–1266.

Logothetis NK, Pauls J, Augath M, Trinath T, Oelterman A (2001): Neurophysiological investigation of the basis of the fMRI signal. Nature 412:150–157.

Long XY, Zuo XN, Kiviniemi V, Yang Y, Zou QH, Zhu CZ, Jiang TZ, Yang H, Gong QY, Wang L, Li KC, Xie S, Zang YF (2008): Default mode network as revealed with multiple methods for resting-state functional MRI analysis. J Neurosci Methods 171:349–355.

Longcamp M, Anton JL, Roth M, Velay JL (2005): Premotor activations in response to visually presented single letters depend on the hand used to write: A study on left-handers. Neuropsychologia 43:1801–1809.

Lund TE, Madsen KH, Sidaros K, Luo WL, Nichols TE (2006): Non-white noise in fMRI: Does modelling have an impact?-Neuroimage 29:54–66.

Ma L, Wang B, Chen X, Xiong J (2007): Detecting functional connectivity in the resting brain: A comparison between ICA and CCA. Magn Reson Imaging 25:47–56.

Malinen S, Hlushchuk Y, Hari R (2007): Towards natural stimulation in fMRI—Issues of data analysis. NeuroImage 35:131–139.

Mantini D, Perrucci MG, Del Gratta C, Romani GL, Corbetta M (2007): Electrophysiological signatures of resting state

networks in the human brain. Proc Natl Acad Sci USA 104: 13170–13175.

McAvoy M, Larson-Prior L, Nolan TS, Vaishnavi SN, Raichle ME, d'Avossa G (2008)Resting states affect spontaneous BOLD oscillations in sensory and paralimbic cortex. J Neurophysiol 100:922–931.

McKeown MJ, Jung TP, Makeig S, Brown G, Kindermann SS, Lee TW, Sejnowski TJ (1998): Spatially independent activity patterns in functional MRI data during the stroop color-naming task. Proc Natl Acad Sci USA 95:803–810.

McKeown MJ, Varadarajan V, Huettel S, McCarthy G (2002): Deterministic and stochastic features of fMRI data: Implications for analysis of event-related experiments. J Neurosci Methods 118:103–113.

Mezer A, Yovel Y, Pasternak O, Gorfine T, Assaf Y (2009): Cluster analysis of resting-state fMRI time series. Neuroimage 45:1117–1125.

Murphy K, Birn RM, Handwerker DA, Jones TB, Bandettini PA (2009): The impact of global signal regression on resting state correlations: Are anti-correlated networks introduced?Neuroimage 44:893–905.

Pawela CP, Biswal BB, Cho YR, Kao DS, Li R, Jones SR, Schulte ML, Matloub HS, Hudetz AG, Hyde JS (2008): Resting-state functional connectivity of the rat brain. Magn Reson Med 59:1021–1029.

Pelled G, Goelman G (2004): Different physiological MRI noise between cortical layers. Magn Res Med 52:913–916

Salvador R, Suckling J, Coleman MR, Pickard JD, Menon D, Bullmore E (2005): Neurophysiological architecture of functional magnetic resonance images of human brain. Cereb Cortex 15:1332–1342.

Schmidhorst VJ, Holland SK (2004): Comparison of three methods for generating group statistical inferences from independent component analysis of functional magnetic resonance imaging data. J Magn Reson Imaging 19:365–368.

Shmuel A, Leopold DA (2008): Neuronal correlates of spontaneous fluctuations in fMRI signals in monkey visual cortex: Implications for functional connectivity at rest. Hum Brain Mapp 29:751–761.

Smith SM (2002): Fast robust automated brain extraction. Hum Brain Mapp 17:143–155.

Sorg C, Riedl V, Mühlau M, Calhoun VD, Eichele T, Läer L, Drzezga A, Förstl H, Kurz A, Zimmer C, Wohlschläger AM (2007): Selective changes of resting-state networks in individuals at risk for Alzheimer's disease. Proc Natl Acad Sci USA 104:18760–18765.

Sridharan D, Levitin DJ, Menon V (2008): A critical role for the right fronto-insular cortex in switching between central-executive and default mode networks. Proc Natl Acad Sci USA 105:12569–12574.

Tohka J, Foerde K, Aron AR, Tom SM, Toga AW, Poldrack RA (2008): Automatic independent component labeling for artifact removal in fMRI. Neuroimage 39:1227–1245.

Uddin LQ, Clare Kelly AM, Biswal BB, Xavier Castellanos F, Milham MP (2009): Functional connectivity of default mode network components: Correlation, anticorrelation, and causality. Hum Brain Mapp 30:625–637.

van de Ven VG, Formisano E, Prvulovic D, Roeder CH, Linden DE (2004): Functional connectivity as revealed by spatial independent component analysis of fMRI measurements during rest. Hum Brain Mapp 22:165–178.

Vincent JL, Patel GH, Fox MD, Snyder AZ, Baker JT, Van Essen DC, Zempel JM, Snyder LH, Corbetta M, Raichle ME (2007): Intrinsic functional architecture in the anaesthetized monkey brain. Nature 447:83–86.